Hydroxylation of indisulam is catalyzed by cytochrome P450 enzymes. The contribution of CYP isoenzymes in CYP-dependent metabolism of indisulam was studied previously using human recombinant isozymes. Taking into account the human liver microsome content of each isozyme (20), it was estimated that CYP2C9 had the highest contribution in indisulam metabolism, followed by CYP2C19 (study report, Eisai Co., Ltd., 2002). Concisely, hydroxylation by CYP2C9 and CYP2C19 may be rate limiting for the metabolism of indisulam.

Polymorphisms in the CYP2C genes may affect the rate of elimination of indisulam. Consequently, treatment outcome may be altered. Furthermore, variant genotypes may be clinically relevant predictors for the risk of severe hematologic toxicity. The purpose of the current study was to evaluate the effect of allelic variants of CYP2C9 and CYP2C19 on indisulam pharmacokinetics in cancer patients.

Materials and Methods

Clinical studies. Indisulam pharmacokinetics have been extensively studied during a phase I program that consisted of seven clinical studies (9–14). Indisulam was administered at various dose levels in 1- or 2-h infusions every 3 weeks (Table 1). Full pharmacokinetic sampling was done during the first treatment cycle, and hematologic parameters were monitored twice weekly. In a pharmacogenetic substudy, which was done in three out of these seven trials, patients were screened for CYP2C allelic variants. Both Caucasian and Japanese patients were included in the substudy because mutant allele frequencies of CYP2C9 were expected to be high in Caucasians and mutant allele frequencies of CYP2C19 were expected to be high in Japanese populations.

Table 1. Patient characteristics and dose levels

	Caucasian	Japanese
Number of patients	46	21
Primary tumor type		
Colorectal carcinoma	9	15
Pancreas carcinoma	10	—
Gastrointestinal carcinoma	3	1
Adenocarcinoma of unknown primary site	7	—
Sarcoma	4	1
Melanoma	2	—
Lung carcinoma	4	3
Renal cell carcinoma	2	—
Ovarian carcinoma	2	—
Other	3	1
Patient characteristics	Median (range)	Median (range)
Male/Female	25/21	15/6
Weight (kg)	74 (43-119)	61 (44-79)
Height (cm)	172 (153-193)	165 (149-180)
Body surface area (m^2)	1.88 (1.36-2.23)	1.68 (1.39-1.94)
Age	59 (19-81)	57 (35-70)
Dose level (mg/m^2)		
350	11 (1-h infusion)	—
400	—	3 (1-h infusion)
500	14 (1-h infusion)	—
600	12 (1-h infusion)	3 (1-h infusion)
700	7 (1-h infusion)	6 (2-h infusion)
800	2 (1-h infusion)	6 (2-h infusion)
900	—	3 (2-h infusion)

The study protocols were approved by medical ethics committees of the centers in which the studies were carried out. Written informed consent was obtained from each patient.

Bioanalysis. Indisulam plasma concentrations of the Caucasian patients were measured using a validated high-performance liquid chromatography (HPLC) method coupled with electrospray ionization tandem mass spectrometry (21). In the Japanese population, concentrations were measured in plasma, plasma ultrafiltrate, and erythrocytes. After sample pretreatment, a validated HPLC method with UV detection was used for quantification of indisulam (14). Both methods were extensively validated and cross-validated according to Food and Drug Administration guidelines (22). Considering the successful cross-validation of the two methods, we did not discriminate between these methods during data analysis.

Genotyping analysis. Pharmacogenetic screening of the Caucasian patients was done for the *2, *3, *4, and *6 mutations of CYP2C9 and for the *2, *3, *4, *5, and *6 polymorphisms of CYP2C19. DNA was isolated from peripheral lymphocytes using the Nucleon BACC kit (Amersham Life Science) and Qiagen kits. Fluorescent allele specific hybridization was used to determine the genotype for CYP2C9*2 and CYP2C9*3. An amplification refractory mutation system (ARMS) was applied for CYP2C19*3 and CYP2C9*5. The remaining mutations were detected by real-time PCR methods. Japanese patients were genotyped for the *2 and *3 mutations of CYP2C9 and CYP2C19 as described by Yamada et al. (14).

Population pharmacogenetic data analysis. Pharmacokinetic data of indisulam were analyzed with a previously developed population pharmacokinetic model using NONMEM (version V, level 1.1; Globomax LLC). The analysis was done using the first-order estimation method in NONMEM after logarithmic data transformation. The population pharmacokinetic model described the distribution and elimination of indisulam for various dosage levels and administration regimens in both Japanese and Caucasian patients (16). The elimination model comprised two parallel pathways: a linear pathway (described by the linear clearance CL) and a saturable Michaelis-Menten pathway (described by a maximal elimination rate, V_{max}, and a Michaelis-Menten constant K_m; ref. 16).

In the current study, the elimination model was extended to evaluate the impact of CYP2C polymorphisms on the pharmacokinetics of indisulam. The relationships between mutations of the CYP2C9 and CYP2C19 genes and each of the three elimination pharmacokinetic parameters (CL, V_{max}, and K_m) were verified.

Allelic variants were incorporated in the population model as covariate relationships according to Eq. A. A pharmacokinetic parameter P had a typical value of P_{pop} in wild-type patients. The typical value of heterozygous patients was equal to P_{pop} reduced by $\theta \times 100\%$. Homozygous mutations were assumed to have twice the impact of heterozygous mutations, and the corresponding typical value of P was reduced by $2 \times \theta \times 100\%$ as compared with wild-type.

$$P = P_{pop} \times (1 - (\theta \times \text{heterozygous} + 2 \times \theta \times \text{homozygous})) \quad (A)$$

Polymorphisms that were observed in the study population at a frequency >2% were tested for their effect on the linear elimination of indisulam (CL) and for their impact on the saturable elimination pathway (V_{max} and/or K_m). Discrimination between models with and without a pharmacogenetic effect was based on the log-likelihood ratio test. A P value of 0.001 was considered statistically significant. This univariate analysis was followed by a multivariate test. After inclusion of the pharmacogenetic relationships that were statistically significant in the univariate analysis, a backward elimination procedure was done. Only effects of allelic variants that were

Table 2. Observed genotype and allele frequencies of the polymorphisms under study

Polymorphism	Nucleotide change (cDNA)	Effect	Caucasian population				Japanese population			
			Wt	Het	Hom	Allele frequency (%)	Wt	Het	Hom	Allele frequency (%)
CYP2C9*2	C430T	R144C	35	10	1	13	21	0	0	0
CYP2C9*3	A1075C	I359L	36	9	1	12	19	2	0	4.8
CYP2C9*5	C1080G	D360E	45	1	0	1.1	21	0	0	0
CYP2C9*6	818 Del A	Frame shift	46	0	0	0	21	0	0	0
CYP2C19*2	G681A	Splicing defect	37	9	0	9.8	10	7	4	36
CYP2C19*3	G636A	W212X	46	0	0	0	18	3	0	7.1
CYP2C19*4	A1G	Initiation codon	45	1	0	1.1	21	0	0	0
CYP2C19*5	C1297T	R433W	46	0	0	0	21	0	0	0
CYP2C19*6	G395A	R132Q	46	0	0	0	21	0	0	0

Abbreviations: Wt, wild type; Het, heterozygous mutant; Hom, homozygous mutant.

significant in the multivariate analysis ($P < 0.001$) were included in the final pharmacokinetic model.

The CYP2C19*2 and CYP2C19*3 mutations were both known to result in nonfunctional protein (23, 24). Therefore, it would not be plausible to expect different effects of these mutations on indisulam metabolism, and consequently, we did not discriminate between these mutations in the statistical analysis.

Covariate relationships between patient characteristics and pharmacokinetic parameters that were previously identified were also included in the extended pharmacogenetic model (16). Hence, the value of V_{max} was not only dependent on genotype, but also on the body surface area. Moreover, the linear clearance was not only dependent on genotype, but also on race. A multivariate analysis was done to verify whether genotype could replace race to explain a difference in CL between Caucasian and Japanese patients.

Assessment of clinical relevance. After establishment of statistically significant pharmacogenetic relationships, the clinical relevance of the effects of polymorphisms were assessed in the study population. The dose-limiting toxicities of indisulam were hematologic side effects such as neutropenia and thrombocytopenia (13). We evaluated the role of CYP2C genotypes in the occurrence of grade 4 neutropenia in the patients who participated in this study. Significant relationships between CYP2C polymorphisms and observed nadir neutrophil counts were identified by the Kruskal-Wallis test using SPSS for Windows (version 11.0.1, SPSS Inc.).

Simulation study of dose-limiting neutropenia. With increasing systemic exposure to indisulam, the risk of dose-limiting hematologic toxicity proved to be increased. A semiphysiologic model of the hematologic toxicity of indisulam has been developed previously (17). This pharmacokinetic-pharmacodynamic model described the time profile of the absolute neutrophil count (ANC) after administration of indisulam. It was used in the current analysis to estimate the risk of dose-limiting neutropenia, defined as an ANC of $< 0.5 \times 10^9$/L during at least 1 week. With this model, patients were simulated to receive the recommended indisulam dosage of 700 mg/m^2. For each patient, the time profile of the ANC was generated, and the occurrence of dose-limiting neutropenia was assessed. First, a group of wild-type patients was simulated. Second, heterozygous and homozygous patient groups were simulated for each polymorphism. Each simulated group consisted of more than 10,000 patients. The risk of dose-limiting neutropenia was defined as the proportion of patients who experienced dose-limiting neutropenia. The relative risk of dose-limiting neutropenia for a variant genotype was the ratio of the proportions in the mutant and the wild-type patient group. The large number of patients in each simulated group guaranteed that the relative risk could be precisely estimated (relative SE <10%).

Dose adaptation. The simulation study as described above was repeated with adapted dosages of indisulam to determine the dose reduction needed to normalize the risk of dose-limiting neutropenia in patients with high-risk CYP2 mutations. This analysis aimed at the development of a straightforward method for dose adaptation, which is feasible for implementation in clinical practice.

Results

Pharmacokinetic samples were obtained from a total of 213 patients. A subpopulation of 21 Japanese and 46 Caucasian patients from three clinical studies was genotyped for polymorphisms in CYP2C9 and CYP2C19 genes. Patient characteristics and administered doses of this subpopulation are listed in Table 1. The variant alleles CYP2C9*2, CYP2C9*3, CYP2C9*5, CYP2C19*2, CYP2C19*3, and CYP2C19*4 were observed in the study population. Genotype frequencies are listed in Table 2. Observed allele frequencies in the current study were consistent with previously reported data in both the Caucasian and the Japanese subpopulation (25–32).

Effect of genomic variants on indisulam exposure. Drug exposure was generally increased in patients with CYP2C9 and/or CYP2C19 mutations, which indicates that indisulam elimination was reduced by some of the CYP2C polymorphisms. This is shown in Fig. 1 for all patients who received 500 mg/m^2 indisulam. Plasma concentration versus time curves show a clear discrimination between mutants (both CYP2C9 and CYP2C19) and wild types at this dose level (Fig. 1A). The area under the concentration-versus-time curve (AUC) were higher for mutants than for wild-type patients (Fig. 1B). Similar plots of other dose levels showed a marked effect of the CYP2C19*2 variant. Patients who were heterozygous for this mutation generally had substantially higher AUC values than wild-type patients. Exposure was further increased in homozygous CYP2C19*2 mutants (data not shown).

To our knowledge, for the first time, the CYP2C9*5 polymorphism was observed in a Caucasian individual. The AUC of indisulam in this patient after administration of 600 mg/m^2 in a 1-h infusion (2,512 mg/L/h) was almost twice higher than the AUC of three wild-type Caucasian patients who had received the same dosage (AUC range 1,035-1,458 mg/L/h).

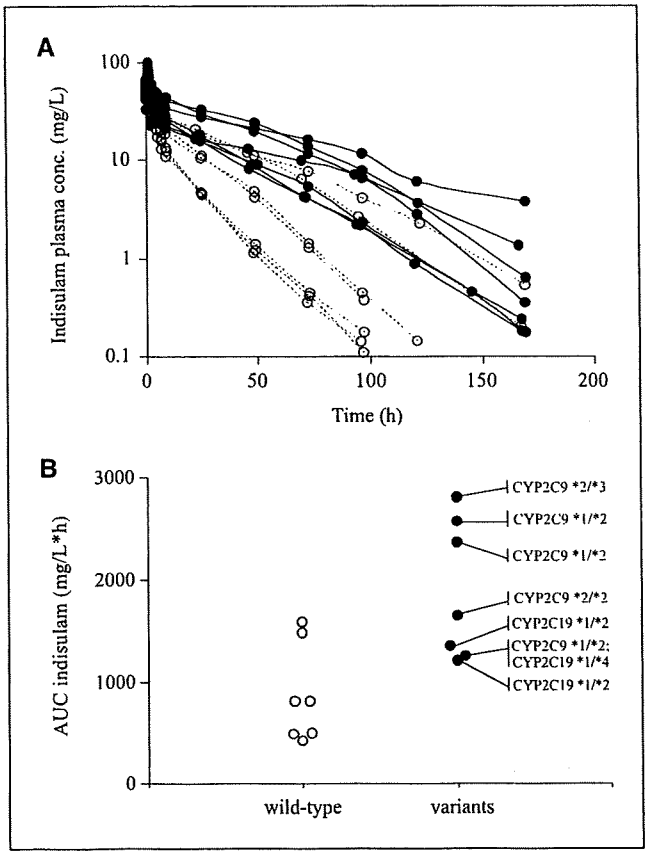

Fig. 1. Plasma concentrations of wild-type patients (—o—) were generally lower than concentrations measured in mutants (—●—). *A*, plasma concentration time curves are depicted of all 14 patients who were treated at the 500 mg/m^2 dose level. *B*, AUC values of the same 14 patients. Variant genotypes are listed (genes not mentioned were wild type).

Population pharmacogenetic data analysis. The CYP2C9*2, CYP2C9*3, CYP2C19*2, and CYP2C19*3 mutations occurred at a frequency >2% and were therefore included in the statistical analysis to evaluate their effect on indisulam pharmacokinetics. In the univariate analysis, the relationships between the CYP2C9*3, CYP2C19*2, and CYP2C19*3 mutations and the Michaelis-Menten elimination rate (V_{max}) were statistically significant. The CYP2C19*2 and CYP2C19*3 polymorphisms also significantly reduced the linear clearance (CL). The Michaelis-Menten constant (K_m) was not significantly affected by any of the polymorphisms.

Upon multivariate evaluation of the univariately selected pharmacogenetic effects, the racial difference in CL was not significantly different from 1 and was therefore excluded from the model. The CYP2C9*3 allelic variant was shown to significantly impair the saturable metabolism of indisulam by a typical 27% reduction of V_{max} in heterozygous mutants ($P < 0.0001$). The relationships between the CYP2C19 mutations and V_{max} were not significant in the multivariate analysis and were excluded during the backward elimination procedure. The CYP2C19*2 and CYP2C19*3 polymorphisms resulted in significant reductions of linear elimination of indisulam ($P < 0.0001$), and the typical value of CL was decreased by 38% in heterozygous patients. The final model included two pharmacogenetic effects: CYP2C9*3 ($\sim V_{max}$) and CYP2C19*2/CYP2C19*3 ($\sim$ CL; Table 3).

Clinical relevance of pharmacogenetic effects. Indisulam clearance was typically reduced in patients with one or more of the genomic variants CYP2C9*3, CYP2C19*2, and CYP2C19*3. Consequently, these patients showed a higher exposure to indisulam. The CYP2C9*3, CYP2C19*2, and CYP2C19*3 polymorphisms were thus expected to cause a higher risk of grade 4 neutropenia.

Data on the occurrence of hematologic toxicity were available for all patients who were included in the pharmacogenetic substudy. Eight patients had grade 4 neutropenia at cycle 1: three Japanese and five Caucasian patients (Fig. 2). Two Japanese patients who received the highest dose level of 900 mg/m^2 indisulam had grade 4 neutropenia. Both patients had the CYP2C19*2 mutation; one patient was homozygous and had a nadir neutrophil count as low as 0.018×10^9/L, and the other patient was heterozygous. A third Japanese patient with a neutrophil count below 0.5×10^9/L was heterozygous for CYP2C19*2 and was treated with 800 mg/m^2 indisulam. Two Caucasian patients had received 800 mg/m^2 indisulam; one was homozygous for the CYP2C9*3 mutation and had severe dose-limiting neutropenia during 2 weeks, whereas the other patient had a wild-type genotype and a neutrophil count below 0.5×10^9/L at a single occasion. Clinical data are depicted in Fig. 2. At the higher dose levels, nadir neutrophil counts decreased with increasing dose level and with an increasing number of influential mutations. Due to small patient numbers, significant relationships between CYP2C polymorphisms and observed nadir neutrophil counts could not be shown. For the same reason, relative risks of severe neutropenia

Table 3. Effect of heterozygous mutations on the pharmacokinetic parameters V_{max} and CL

Polymorphism	Effect	Effect size (%)	95% CI* (%)	P†
CYP2C9*2	No significant effect			
CYP2C9*3	Reduction of V_{max}	27	13-40	<0.0001
CYP2C9*5	Insufficient data			
CYP2C19*2	Reduction of CL	38	31-45	<0.0001
CYP2C19*3				
CYP2C19*4	Insufficient data			

*The 95% confidence interval was established by likelihood profiling.
† The log-likelihood ratio test was used to calculate the *P* value.

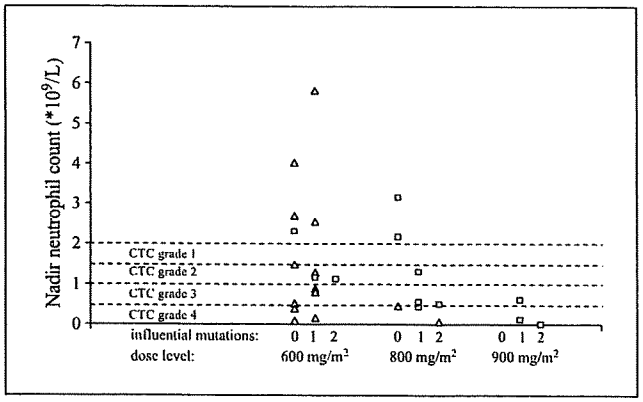

Fig. 2. Grade 4 neutropenia at cycle 1 was observed at dose levels 600, 800, and 900 mg/m^2. Nadir neutrophil counts of patients who were treated at these dose levels are plotted versus the number of influential mutations, i.e., the combined number of CYP2C9*3, CYP2C19*2, and CYP2C19*3 mutations. (△, Caucasian patients; □, Japanese patients).

for the various mutations could not adequately be determined using clinical data.

Simulation study of dose-limiting neutropenia. The hypothesis that CYP2C9*3, CYP2C19*2, and CYP2C19*3 polymorphisms may cause a higher risk of dose-limiting neutropenia was confirmed by the results of the simulation study listed in Table 4. These results show that the risk of dose-limiting neutropenia was increased by 40% or more in simulated patient groups with a single polymorphism. Homozygous mutations or combinations of multiple heterozygous mutations may result in a relative risk of serious toxicity of more than 2.

Dose adaptation. The CYP2C19*2 and CYP2C19*3 mutations caused a larger increase of the risk of dose-limiting neutropenia than CYP2C9*3. Consequently, the dosage of indisulam should be adapted to a larger extent for CYP2C19*2 and CYP2C19*3 than for CYP2C9*3. Each CYP2C19 mutation required a dose reduction of 100 mg/m^2. The recommended dose reduction for a CYP2C9*3 mutation was 50 mg/m^2. A simulation study showed that this guidance for dose adaptation resulted in the normalization of the relative risk of severe neutropenia (Table 4).

Discussion

In the current study, the relationships between various polymorphisms of two CYP450 enzymes (CYP2C9 and CYP2C19) and the pharmacokinetics of indisulam were assessed. It was shown that the elimination rate of indisulam was significantly decreased by CYP2C9*3, CYP2C19*2, and CYP2C19*3 polymorphisms. These CYP2C mutations caused an increased risk of dose-limiting neutropenia.

The activity of the *3-mutated CYP2C9 enzyme was shown to be reduced for *S*-warfarin *in vitro* by Haining et al. (33). This polymorphism was also associated to poor tolbutamide metabolism *in vivo* (34). In the current pharmacogenetic study, the *3 mutation in the CYP2C9 gene reduced the Michaelis-Menten elimination rate of indisulam. Thus, the saturable elimination pathway may correspond to hydroxylation of indisulam by CYP2C9 (19).

De Morais et al. (23, 24) showed that the *2 and *3 mutations in the CYP2C19 gene created a premature stop codon, resulting in a truncated nonfunctional CYP2C19 protein. These CYP2C19 mutations were related to poor metabolism of the CYP2C19 substrate (*S*)-mephenytoin (23, 24) and to a reduction of the clearance of indisulam. Consequently, the linear elimination pathway of indisulam may represent hydroxylation by CYP2C19 (19).

The CYP2C9*5 mutation results in lower enzymatic activity and that CYP2C19*4 represents a defective allele (30, 35). Therefore, the CYP2C9*5 and CYP2C19*4 polymorphisms may be related to reduced indisulam clearance. The AUC of indisulam in a patient who was heterozygous for the CYP2C9*5 mutation was indeed substantially higher than the AUC of three Caucasian wild-type patients who had received the same indisulam dose. Due to low allelic frequency, statistical significance of the effects of the CYP2C9*5 and CYP2C19*4 polymorphisms could not be shown in the present study.

In our population of Japanese and Caucasian patients, six CYP2C polymorphisms were observed, which are located on chromosome 10. The occurrence of multiple polymorphisms on the same allele is indicated by the haplotype. Multiple polymorphisms may not be fully independent. It may therefore be preferable to consider the haplotype rather than the genotype of individual polymorphisms for data analysis. This

Table 4. Simulated relative risk of dose-limiting neutropenia after administration of indisulam in a 1-h infusion and the 95% confidence intervals (in brackets)

Polymorphism	Caucasian heterozygous	Homozygous	Japanese heterozygous	Homozygous
Standard dose: 700 mg/m^2				
CYP2C9*3	1.39 (1.21-1.77)	2.24 (1.45-3.27)	1.47 (1.11-1.60)	NA
CYP2C19*2	1.86 (1.69-2.08)	NA	1.97 (1.73-2.33)	4.51 (3.31-6.25)
CYP2C19*3				
Adjusted dose: 700 mg/m^2—recommended dose reduction				
CYP2C9*3	1.03 (0.82-1.29)	1.30 (0.81-2.18)	1.09 (0.79-1.24)	NA
CYP2C19*2	1.04 (0.78-1.06)	NA	1.07 (0.86-1.20)	1.01 (0.69-1.62)
CYP2C19*3				

NOTE: Each subpopulation consisted of at least 10,000 simulated patients. These genotypes were not observed in the study population.
Abbreviation: NA, not applicable.

strategy was, however, not suitable for the current analysis because haplotype frequencies were too low.

The CYP2C19 polymorphisms occurred at much higher frequencies in the Japanese population compared with the Caucasian population (CYP2C19*2: 36% versus 9.8%; CYP2C19*3: 7.1% versus 0%). Because these CYP2C19 variants significantly impaired indisulam clearance, Japanese patients typically have a lower CL than Caucasians. Indeed, in the previously published population pharmacokinetic model, Japanese patients had a 3.4-fold lower value for CL than Caucasian individuals (16). This difference was not statistically significant upon inclusion of CYP2C19 genotype in the drug elimination model. This confirms that the lower linear clearance of indisulam in Japanese patients is due to genomic differences between the Caucasian and Japanese patient populations.

Mixed-effects modeling was used to assess the effects of CYP2C mutations on pharmacokinetic parameters. From a statistical standpoint, this method is superior to more commonly used methods in pharmacogenetic studies, where standard pharmacokinetic two-stage analyses are followed by conventional statistical tests in order assess differences between genetic subgroups (36).

It was shown that CYP2C9*3, CYP2C19*2, and CYP2C19*3 mutations led to decreased indisulam clearance and increased drug exposure. A clear relationship has been established between indisulam pharmacokinetics and its dose-limiting toxicities, neutropenia and thrombocytopenia. Based on the results of the present pharmacogenetic study and a semi-physiologic pharmacokinetic-pharmacodynamic model, it was expected that the risk of hematologic side effects is higher for patients with variant CYP2C9 and/or CYP2C19 alleles than for wild-type patients. A simulation study showed that the relative risk of dose-limiting neutropenia may be 2.2 for a homozygous Caucasian CYP2C9*3 mutant and 4.5 for a homozygous Japanese CYP2C19*2 mutant after administration of the recommended dosage of 700 mg/m^2 indisulam. Patient groups in the study population were too small to verify these estimated relative risks of dose-limiting neutropenia with observed data on hematologic toxicity. Nevertheless, the current clinical data imply that the CYP2C9*3 polymorphism is predictive for the occurrence of hematologic toxicity: the relative risk of grade 4 neutropenia was 2 in a group of 12 patients who were treated at the 600 mg/m^2 dose level and a patient with a homozygous CYP2C9*3 genotype had more severe neutropenia than a wild-type patient after administration of 800 mg/m^2. Furthermore, the lowest neutrophil nadir was observed in a Japanese homozygous CYP2C19*2 mutant patient.

The pharmacogenetic effects may be relevant for the treatment of patients with indisulam. Pretreatment genetic screening will permit planning of appropriate initial dosing for individual patients to achieve an optimal therapeutic effect. A reduced initial dosage for patients with high-risk CYP2C mutations is recommended. This recommendation is based on a retrospective study of limited sample size and should therefore be carefully interpreted. Haplotype frequencies in the study population were insufficient to provide a dosing strategy for patients with variant alleles of both CYP2C9 and CYP2C19.

In conclusion, CYP2C9*3, CYP2C19*2, and CYP2C19*3 polymorphisms were related to a decreased elimination rate of indisulam. Screening for these CYP2C polymorphisms may assist in the selection of an optimized initial indisulam dosage. It seems warranted to perform a prospective study to define solid recommendations for pharmacogenetically guided dose adjustments.

Acknowledgments

We thank Sanae Yasuda for her critical review of the manuscript.

References

1. Fukuoka K, Usuda J, Iwamoto Y, et al. Mechanisms of action of the novel sulfonamide anticancer agent E7070 on cell cycle progression in human non – small cell lung cancer cells. Invest New Drugs 2001;19: 219–27.
2. van Kesteren C, Beijnen JH, Schellens JHM. E7070: a novel synthetic sulfonamide targeting the cell cycle progression for the treatment of cancer. Anticancer Drugs 2002;13:989–97.
3. Haddad RI, Weinstein LJ, Wieczorek TJ, et al. A phase II clinical and pharmacodynamic study of E7070 in patients with metastatic, recurrent, or refractory squamous cell carcinoma of the head and neck: modulation of retinoblastoma protein phosphorylation by a novel chloroindolyl sulfonamide cell cycle inhibitor. Clin Cancer Res 2004;10:4680–7.
4. Raftopoulos H, Escudier B, Renshaw G, et al.: A phase II multicenter study of the cyclin-dependent kinase inhibitor indisulam in patients with inoperable and/or metastatic renal cell carcinoma (RCC) [abstract]. J Clin Oncol – American Society of Clinical Oncology Annual Meeting Proceedings (Post-Meeting Edition) 2004;22:414s.
5. Smyth JF, Aamdal S, Awada A, et al. Phase II study of E7070 in patients with metastatic melanoma. Ann Oncol 2005;16:158–61.
6. Fumoleau P, Viens P, Cottu PH, et al. A multi center phase II study of E7070, a chloroindolyl-sulfonamide anticancer agent in anthracycline and taxane pre treated breast cancer [abstract]. 26th San Antonio Breast Cancer Symposium 2003.
7. Talbot DC, Norbury C, Slade M, et al. A phase II and pharmacodynamic study of E7070 in patients with non – small cell lung cancer (NSCLC) who have failed platinum-based chemotherapy [abstract]. Proc Am Soc Clin Oncol 2002;21:327a.
8. Mainwaring PN, Van Cutsem E, Van Laethem JL, et al. A multicentre randomised phase II study of E7070 in patients with colorectal cancer who have failed 5-fluorouracil – based chemotherapy [abstract]. Proc Am Soc Clin Oncol 2002;21:153a.
9. Raymond E, ten Bokkel Huinink WW, Taieb J, et al. Phase I and pharmacokinetic study of E7070, a novel chloroindolyl sulfonamide cell-cycle inhibitor, administered as a one-hour infusion every three weeks in patients with advanced cancer. J Clin Oncol 2002; 20:3508–21.
10. Punt CJA, Fumoleau P, van de Walle B, Faber MN, Ravic M, Campone M. Phase I and pharmacokinetic study of E7070, a novel sulfonamide, given at a daily times five schedule in patients with solid tumors. A study by the EORTC-early clinical studies group (ECSG). Ann Oncol 2001;12:1289–93.
11. Terret C, Zanetta S, Roche H, et al. Phase I clinical and pharmacokinetic study of E7070, a novel sulfonamide given as a 5-day continuous infusion repeated every 3 weeks in patients with solid tumours. A study by the EORTC Early Clinical Study Group (ECSG). Eur J Cancer 2003;39:1097–104.
12. Dittrich C, Dumez H, Calvert H, et al. Phase I and pharmacokinetic study of E7070, a chloroindolyl-sulfonamide anticancer agent, administered on a weekly schedule to patients with solid tumors. Clin Cancer Res 2003;9:5195–204.
13. Raymond E, Fumoleau P, Roche H, et al. Combined results of 4 phase I and pharmacokinetic studies of E7070, a novel chloroindoly-sulphonamide inhibiting the activation of cdk2 and cyclin E [abstract]. Clin Cancer Res 2000;6:4529s.
14. Yamada Y, Yamamoto N, Shimoyama T, et al. Phase I pharmacokinetic and pharmacogenomic study of E7070 administered once every 21 days. Cancer Sci 2005;96:721–8.
15. van Kesteren C, Mathôt RAA, Raymond E, et al. Population pharmacokinetics of the novel anticancer agent E7070 during four phase I studies: model building and validation. J Clin Oncol 2002;20: 4065–73.
16. Zandvliet AS, Schellens JHM, Copalu W, Beijnen JH, Huitema ADR. A semi-physiological population pharmacokinetic model describing the non-linear disposition of indisulam. J Pharmacokinet Pharmacodyn 2006;33:543–70.
17. van Kesteren C, Zandvliet AS, Karlsson MO, et al. Semi-physiological model describing the hematological toxicity of the anti-cancer agent indisulam. Invest New Drugs 2005;23:225–34.
18. van den Bongard HJGD, Pluim D, Rosing H, et al. An excretion balance and pharmacokinetic study of the novel anticancer agent E7070 in cancer patients. Anticancer Drugs 2002;13:807–14.
19. Beumer JH, Hillebrand MJX, Pluim D, et al. Human metabolism of [(14)C]indisulam following i.v.

infusion in cancer patients. Invest New Drugs 2005; 23:317–30.
20. Rodrigues AD. Integrated cytochrome P450 reaction phenotyping: attempting to bridge the gap between cDNA-expressed cytochromes P450 and native human liver microsomes. Biochem Pharmacol 1999;57:465–80.
21. Beumer JH, Rosing H, Hillebrand MJX, et al. Quantitative determination of the novel anticancer drug E7070 (indisulam) and its metabolite (1,4-benzene disulphonamide) in human plasma, urine and faeces by high-performance liquid chromatography coupled with electrospray ionization tandem mass spectrometry. Rapid Commun Mass Spectrom 2004;18:2839–48.
22. U.S. Department of Health and Human Services, Food and Drug Administration, Center for Drug Evaluation and Research (CDER). Guidance for Industry: Bioanalytical Method Validation. 2001.
23. De Morais SM, Wilkinson GR, Blaisdell J, Meyer UA, Nakamura K, Goldstein JA. Identification of a new genetic defect responsible for the polymorphism of (*S*)-mephenytoin metabolism in Japanese. Mol Pharmacol 1994;46:594–8.
24. De Morais SM, Wilkinson GR, Blaisdell J, Nakamura K, Meyer UA, Goldstein JA. The major genetic defect responsible for the polymorphism of *S*-mephenytoin metabolism in humans. J Biol Chem 1994;269: 15419–22.
25. Xie HG, Prasad HC, Kim RB, Stein CM. CYP2C9 allelic variants: ethnic distribution and functional significance. Adv Drug Deliv Rev 2002;54:1257–70.
26. Allabi AC, Gala JL, Desager JP, Heusterspreute M, Horsmans Y. Genetic polymorphisms of CYP2C9 and CYP2C19 in the Beninese and Belgian populations. Br J Clin Pharmacol 2003;56:653–7.
27. Kidd RS, Curry TB, Gallagher S, Edeki T, Blaisdell J, Goldstein JA. Identification of a null allele of CYP2C9 in an African-American exhibiting toxicity to phenytoin. Pharmacogenetics 2001;11:803–8.
28. Xie HG, Stein CM, Kim RB, Wilkinson GR, Flockhart DA, Wood AJ. Allelic, genotypic and phenotypic distributions of *S*-mephenytoin 4′-hydroxylase (CYP2C19) in healthy Caucasian populations of European descent throughout the world. Pharmacogenetics 1999;9: 539–49.
29. Goldstein JA, Ishizaki T, Chiba K, et al. Frequencies of the defective CYP2C19 alleles responsible for the mephenytoin poor metabolizer phenotype in various Oriental, Caucasian, Saudi Arabian and American black populations. Pharmacogenetics 1997;7:59–64.
30. Ferguson RJ, De Morais SM, Benhamou S, et al. A new genetic defect in human CYP2C19: mutation of the initiation codon is responsible for poor metabolism of *S*-mephenytoin. J Pharmacol Exp Ther 1998;284: 356–61.
31. Xiao ZS, Goldstein JA, Xie HG, et al. Differences in the incidence of the CYP2C19 polymorphism affecting the *S*-mephenytoin phenotype in Chinese Han and Bai populations and identification of a new rare CYP2C19 mutant allele. J Pharmacol Exp Ther 1997; 281:604–9.
32. Ibeanu GC, Goldstein JA, Meyer U, et al. Identification of new human CYP2C19 alleles (CYP2C19*6 and CYP2C19*2B) in a Caucasian poor metabolizer of mephenytoin. J Pharmacol Exp Ther 1998;286: 1490–5.
33. Haining RL, Hunter AP, Veronese ME, Trager WF, Rettie AE. Allelic variants of human cytochrome P450 2C9: baculovirus-mediated expression, purification, structural characterization, substrate stereoselectivity, and prochiral selectivity of the wild-type and I359L mutant forms. Arch Biochem Biophys 1996;333: 447–58.
34. Sullivan-Klose TH, Ghanayem BI, Bell DA, et al. The role of the CYP2C9–359 allelic variant in the tolbutamide polymorphism. Pharmacogenetics 1996;6: 341–9.
35. Dickmann LJ, Rettie AE, Kneller MB, et al. Identification and functional characterization of a new CYP2C9 variant (CYP2C9*5) expressed among African Americans. Mol Pharmacol 2001;60:382–7.
36. Ette EI, Williams PJ. Population pharmacokinetics I: background, concepts, and models. Ann Pharmacother 2004;38:1702–6.

original article

Annals of Oncology 21: 255–262, 2010
doi:10.1093/annonc/mdp304
Published online 24 July 2009

Association between gain-of-function mutations in *PIK3CA* and resistance to HER2-targeted agents in *HER2*-amplified breast cancer cell lines

Y. Kataoka[1], T. Mukohara[2,3]*, H. Shimada[4], N. Saijo[4], M. Hirai[1] & H. Minami[2,3]

[1]*Hospital Pharmacy;* [2]*Cancer Center, Kobe University Hospital;* [3]*Medical Oncology, Department of Medicine, Kobe University Graduate School of Medicine, Chuo-ku, Kobe and* [4]*Research Center for Innovative Oncology, National Cancer Hospital East, Kashiwa, Japan*

Received 24 April 2009; accepted 4 May 2009

Background: The mechanism of resistance to human epidermal growth factor receptor 2 (HER2)-targeted agents has not been fully understood. We investigated the influence of *PIK3CA* mutations on sensitivity to HER2-targeted agents in naturally derived breast cancer cells.

Materials and methods: We examined the effects of Calbiochem (CL)-387,785, HER2 tyrosine kinase inhibitor, and trastuzumab on cell growth and *HER2* signaling in eight breast cancer cell lines showing *HER2* amplification and trastuzumab-conditioned BT474 (BT474-TR).

Results: Four cell lines with *PIK3CA* mutations (E545K and H1047R) were more resistant to trastuzumab than the remaining four without mutations (mean percentage of control with 10 μg/ml trastuzumab: 58% versus 92%; $P = 0.010$). While *PIK3CA*-mutant cells were more resistant to CL-387,785 than *PIK3CA*-wild-type cells (mean percentage of control with 1 μM CL-387,785: 21% versus 77%; $P = 0.001$), CL-387,785 retained activity against BT474-TR. Growth inhibition by trastuzumab and CL-387,785 was more closely correlated with changes in phosphorylation of S6K (correlation coefficient, 0.811) than those of HER2, Akt, or ERK1/2. Growth of most *HER2*-amplified cells was inhibited by LY294002, regardless of *PIK3CA* genotype.

Conclusions: *PIK3CA* mutations are associated with resistance to HER2-targeted agents. PI3K inhibitors are potentially effective in overcoming trastuzumab resistance caused by *PIK3CA* mutations. S6K phosphorylation is a possibly useful pharmacodynamic marker in HER2-targeted therapy.

Key words: breast cancer, HER2, *PIK3CA*, trastuzumab

introduction

Breast cancer is the leading cause of cancer death among women worldwide, with ~1 million new cases reported each year [1, 2]. Approximately 20% of breast cancer tumors show overexpression of the HER2 protein, which is mainly caused by gene amplification. HER2 overexpression has been repeatedly identified as a poor prognostic factor [3, 4]. Trastuzumab is a humanized mAb targeting the extracellular domain of the HER2 protein. From the late 1990s, clinical studies have intensively evaluated the therapeutic roles of trastuzumab. For the treatment of HER2-overexpressing metastatic breast cancers, studies report that a combination of trastuzumab and conventional chemotherapy shows significantly higher efficacy than chemotherapy alone [5]. The use of trastuzumab has extended to the treatment of operable HER2-overexpressing breast cancer as an adjuvant or neoadjuvant [6–8]. Despite promising usefulness in clinics, a modest percentage of patients are reported to benefit from trastuzumab therapy, with response rates to trastuzumab as a single agent of ~20% [9]. In addition, even when trastuzumab therapy leads to temporary tumor shrinkage, clinical relapse is observed for the vast majority of metastatic patients. To develop adequate therapies capable of overcoming primary and secondary resistance to trastuzumab, a better understanding of the resistance mechanism is crucial.

To date, several mechanisms of primary resistance to trastuzumab have been proposed. A series of studies indicated that trastuzumab resistance is due to the truncated form of HER2, which lacks an extracellular domain to which trastuzumab is indicated to attach [10, 11]. Nagata et al. [12] demonstrated that loss of phosphatase and tensin homolog deleted on chromosome 10 (PTEN), a negative regulator of PI3K, correlates with poor response to trastuzumab. More recently, the roles of *PIK3CA* in trastuzumab resistance have been under particular investigation. Somatic mutations of *PIK3CA* were first identified in 2004 in various malignant tumors including breast cancer [13]. Subsequent studies have reported that the E545K and H1047R hotspot mutations, found

Correspondence to: Dr T. Mukohara, Department of Medical Oncology, Kobe University Hospital, 7-5-2, Kusunoki-cho, Chuo-ku, Kobe 650-0017, Japan. Tel: +81-78-382-5825; Fax: +81-78-382-5821; E-mail: mukohara@med.kobe-u.ac.jp

on exons 9 and 20, respectively, are the most frequent types of mutation, found in 8%–40% of breast cancer tumors [13–16]. Both hotspot mutations are gain-of-function mutations which transform normal mammary epithelial cells [17, 18]. Berns et al. [19] investigated the roles of gain-of-function mutations of the *PIK3CA* gene in trastuzumab resistance by transfecting wild-type and mutant (H1047R) forms of *PIK3CA* in SKBR-3 HER2-overexpressing breast cancer cells. Results showed that compared with green fluorescent protein (GFP) control, both wild-type and mutant *PIK3CA* transfections resulted in trastuzumab resistance. Further, analysis of *PIK3CA* genotypes in tumor samples obtained from breast cancer patients having undergone trastuzumab-based therapy showed an association between the presence of *PIK3CA* hotspot mutations and shorter time to progression after therapy [19].

Tyrosine kinase inhibitors (TKIs) have also been investigated as potential agents against trastuzumab resistance [20]. A clinical study in metastatic breast cancer patients having previously experienced tumor progression under trastuzumab-based therapies showed that compared with capecitabine alone, treatment using a combination of capecitabine with lapatinib, a dual inhibitor of epidermal growth factor receptor (EGFR) and HER2 tyrosine kinase, lead to significantly longer time to progression [21]. Eichhorn et al. [22], however, demonstrated that transfection of mutant *PIK3CA* (H1047R) in BT474 HER2-overexpressing breast cancer cells resulted in resistance to lapatinib compared with parental cells. Further, results showed that resistance was overcome using NVP-BEZ235, a PI3K and mammalian target of rapamycin dual inhibitor [22].

These findings based on gene manipulations indicate that gain-of-function mutations in the *PIK3CA* gene lead to resistance to trastuzumab, as well as HER2-TKI. To our knowledge, however, these findings have not been confirmed in naturally derived breast cancer cells. Here, trastuzumab resistance due to *PIK3CA* mutations was evaluated in eight naturally derived breast cancer cell lines harboring *HER2* gene amplification. Further, possible therapeutic means to overcome primary and secondary resistance to trastuzumab were investigated, as well as potential pharmacodynamic markers correlated with the growth-inhibitory effect of HER2-targeted drugs.

materials and methods

cell culture

MCF-7, MDA-MB-361, HCC1954, MDA-MB-453, UACC893, CAMA-1, MDA-MB-435S, MDA-MB-415, ZR75-30, HCC70, MDA-MB-468, and HCC1419 cell lines were purchased from the American Type Culture Collection (Manassas, VA). BT474, SKBR-3, BT549, T47D, ZR75-1, and MDA-MB-231 cells were kindly provided by Ian Krop of the Dana-Farber Cancer Institute. Of the 18 breast cancer cell lines, eight (ZR75-30, BT474, SKBR-3, HCC1419, MDA-MB-453, MDA-MB-361, HCC1954, and UACC 893) were reported to have *HER2* gene amplification [23], with levels of PTEN protein expression equivalent to those reported in our previous study [24]. Among the *HER2*-amplified cell lines, ZR75-30, SKBR-3, and HCC1419 were reported to contain the wild-type *PIK3CA* gene and MDA-MB-453, MDA-MB-361, HCC1954, and UACC893 hotspot *PIK3CA* mutations (Table 1) [14]. BT474 was reported to contain a relatively rare type of *PIK3CA* mutation at exon 2, K111N (Table 1) [14]. MDA-MB-435S, MDA-MB-468, and MDA-MB-231 cells were maintained in Dulbecco's Modified Eagle's Medium (Cellgro; Mediatech, Inc., Herndon, CA) with 10% fetal bovine serum (FBS) (Gemini Bio-Products, Inc., Woodland, CA), 100 U/ml penicillin, 100 U/ml streptomycin, and 2 mM glutamine. The remaining cell lines were maintained in RPMI-1640 medium (Cellgro; Mediatech, Inc.) supplemented with 10% FBS, 100 U/ml penicillin, 100 U/ml streptomycin, and 2 mM glutamine. All cells were grown at 37°C in a humidified atmosphere with 5% CO_2 and were in logarithmic growth phase at initiation of the experiments.

Table 1. Genotype of *PIK3CA* in *HER2*-amplified breast cancer cell lines

Cell line	Genotype of *PIK3CA*
BT474	K111N
ZR75-30	wt
SKBR-3	wt
HCC1419	wt
MDA-MB-361	E545K
MDA-MB-453	H1047R
HCC1954	H1047R
UACC893	H1047R

wt, wild-type.

drugs

Trastuzumab was obtained from the Kobe University Hospital pharmacy. CL-387,785, a dual inhibitor of EGFR and HER2 [25], and LY294002, a PI3K inhibitor, were purchased from Calbiochem (San Diego, CA). Stock solutions were prepared in dimethyl sulfoxide (DMSO) and stored at −20°C. Before each experiment, drugs were diluted in fresh media. The final DMSO concentration was <0.1% for all experiments.

antibodies and western blotting

Cells were washed with ice-cold phosphate-buffered saline and scraped immediately after adding lysis buffer [20 mM Tris (pH 7.5), 150 mM NaCl, 10% glycerol, 1% Nonidet P-40, and 2 mM EDTA] containing protease and phosphatase inhibitors (100 mM NaF, 1 mM phenylmethylsulfonyl fluoride, 1 mM Na_3VO_4, 2 μg/ml aprotinin, and 5 μg/ml leupeptin). Lysates were centrifuged at 14 000 relative centrifugal force for 10 min. Supernatants were collected as protein extract and then separated by electrophoresis on 7.6% polyacrylamide–sodium dodecyl sulfate gels, followed by transfer to nitrocellulose membranes (Millipore Corporate Headquarters, Billerica, MA) and detection by immunoblotting using an enhanced chemiluminescence system (New England Nuclear Life Science Products, Inc., Boston, MA). The resulting signals were digitally quantified using the ImageJ software (www.nih.gov). Phospho-HER2/ErbB2 (Thr1221/1222), phospho-p70 S6 Kinase (Thr389), phospho-Akt (Ser473)(D9E), and PathScan(R) Multiplex Western Cocktail I were purchased from Cell Signaling Technology (Beverly, MA). The phospho-1/2 (pT185/pY187) antibody was purchased from Biosource International Inc. (Camarillo, CA), the c-erbb-2 antibody from Chemicon (Billerica, MA), and β-actin antibody from Sigma-Aldrich (St Louis, MO).

cell growth assay

Growth inhibition was assessed using the 3-(4,5-dimethylthiazol-2-yl)-5-(3-carboxymethoxyphenyl)-2-(4-sulfophenyl)-2H-tetrazolium (MTS) assay (Promega, Madison, WI), a colorimetric method for determining the number of viable cells based on the bioreduction of MTS to a soluble formazan product, which is detectable by spectrophotometry at a wavelength of 490 nm. Cells were diluted in 160 μl/well of maintenance cell culture media and plated in 96-well flat-bottom plates (Corning, Inc., Corning, NY). After a 96-h growth period, the number of cells required to obtain an absorbance of 1.3–2.2, the linear range of the assay, was

determined for each cell line beforehand. The number of cells per well used in the subsequent experiments were as follows: MCF-7, 2000; MDA-MB-361, 8000; HCC1954, 2500; MDA-MB-453, 7000; UACC893, 7500; CAMA-1, 6000; MDA-MB-435S, 2000; ZR75-30, 7500; HCC70, 4000; HCC1419, 8000; BT474, 3000; SKBR-3, 2500; BT549, 2000; T47D, 2500; ZR75-1, 7500; MDA-MB-415, 5000; and MDA-MB-231, 2500. At 24 h after plating, cell culture media were replaced with 10% FBS-containing media with and without trastuzumab or CL-387,785, followed by incubation for an additional 120 h. Trastuzumab and CL-387,785 concentrations ranged from 33 ng/ml to 100 μg/ml and from 3.3 nM to 10 μM, respectively. A total of 6–12 plate wells were set for each experimental point, and all experiments were carried out at least in triplicate. Data are expressed as percentage of growth relative to that of untreated control cells.

generation of *in vitro* BT474-TR

To generate a cell line resistant to trastuzumab, BT474 cells were continuously exposed to 100 μg/ml trastuzumab. To confirm the emergence of resistant clones, MTS assays were carried out every five passages after allowing cells to grow in drug-free conditions for at least 4 days. After 11 months of drug exposure, cells showed sufficient resistance (Figure 1) and were designated as BT474-TR. For controls, BT474 parental cells were concomitantly maintained without trastuzumab, and drug sensitivity was compared with trastuzumab-conditioned cells. No significant change in the sensitivity to trastuzumab was observed in parental cells during the drug-exposure period (data not shown).

results

inhibitory effect of trastuzumab on growth in breast cancer cell lines

We first screened 17 breast cancer cell lines for *in vitro* growth inhibition using trastuzumab. We confirmed that all relatively sensitive cell lines were *HER2*-amplified (Figure 2A). Among eight *HER2*-amplified cell lines, those with hotspot mutations in *PIK3CA* appeared resistant compared with the remaining cell lines (Figure 2B and C). We categorized BT474 as a *PIK3CA*-wild-type cell line in this study, based on reports showing that the K111N mutation lack ability of transformation and its influence on downstream signaling is negligible [18, 26]. A significant difference in sensitivity at 10 μg/ml trastuzumab was observed between *PIK3CA*-wild-type and -mutant cells (Figure 2C; $P = 0.010$). Protein expression levels of p110-α, the product of *PIK3CA*, were not correlated with sensitivity to trastuzumab (Figure 2C).

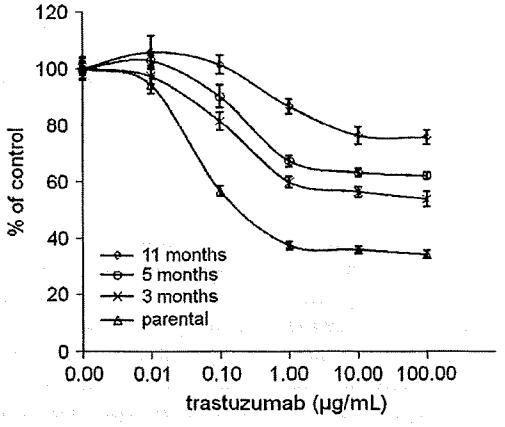

Figure 1. Development of BT474-TR. BT474 cells were continuously exposed to 100 μg/ml trastuzumab. BT-474 and trastuzumab-conditioned BT474 cells were grown in 10% serum-containing media for 5 days in the presence of various concentrations of trastuzumab. The percentage of viable cells is shown relative to that of the untreated control and plotted on the *y*-axis, whereas trastuzumab concentrations are plotted on the *x*-axis. Each data point represents the mean value and standard deviation of 6–12 replicate wells. Trastuzumab resistance increased in cells in a time-dependent manner. After 11 months, cells were designated as BT474-TR.

association between *PIK3CA* mutations and HER2-TKI resistance

Lapatinib, a HER2-TKI which may potentially overcome trastuzumab resistance, has been used in clinical settings [21]. We therefore tested a commercially available HER2-TKI, CL-387,785 [25], on *HER2*-amplified breast cancer cells. As shown in Figure 2D, cell lines with hotspot *PIK3CA* mutations showed resistance to CL-387,785. A statistically significant difference in sensitivity to 1 μM CL-387,785 was observed between *PIK3CA*-wild-type and -mutant cells (Figure 2C; $P = 0.001$) [24].

We then established a trastuzumab-resistant BT474 cell line (BT474-TR), a model of secondary resistant cells, by continuous exposure to trastuzumab (see 'Materials and methods' section). In contrast to *PIK3CA*-mutant cells, which showed primary resistance to trastuzumab, BT474-TR cells remained sensitive to CL-387,785 (Figure 3), which indicates that secondary resistant cells maintain dependency on HER2 signaling for growth.

association between phosphorylation change in S6K and growth inhibition by HER2-targeted agents

To identify potential pharmacodynamic markers of sensitivity to HER2-targeted therapy, we examined changes in phosphorylation of HER2 and representative downstream signaling molecules in 10% FBS-containing media with or without 10 μg/ml trastuzumab or 1 μM CL-387,785 (Figure 4A). The trastuzumab concentration was selected based on maintained growth inhibition (Figure 2B) and wide use in previous studies [11, 19]. The 1-μM CL-387,785 concentration was selected based on the approximate maximum plasma concentration of most TKIs available in clinics to date, including lapatinib [27], and use in previous studies [28, 29].

Trastuzumab treatment resulted in moderate phosphorylation inhibition of Akt and/or S6K in cell lines with wild-type *PIK3CA*. In contrast, no significant changes in Akt and S6K phosphorylation were observed in cell lines with hotspot mutant *PIK3CA*, as well as in BT474-TR cells. Although in ZR75-30, trastuzumab treatment appeared to inhibit phospho-ERK1/2, no significant changes were observed in other sensitive cells, namely BT474 and SKBR-3 (Figure 4A). In addition, phospho-ERK1/2 levels increased in MDA-MB-361 and UACC893, which indicates the presence of compensational cell signaling. Further, with the exception of HCC1419, treatment with CL-387,785 resulted in significant inhibition of Akt and S6K phosphorylation in BT474-TR and *PIK3CA*-wild-type cells, whereas residual phosphorylation signals were observed in all *PIK3CA* hotspot mutant cells.

doi:10.1093/annonc/mdp304

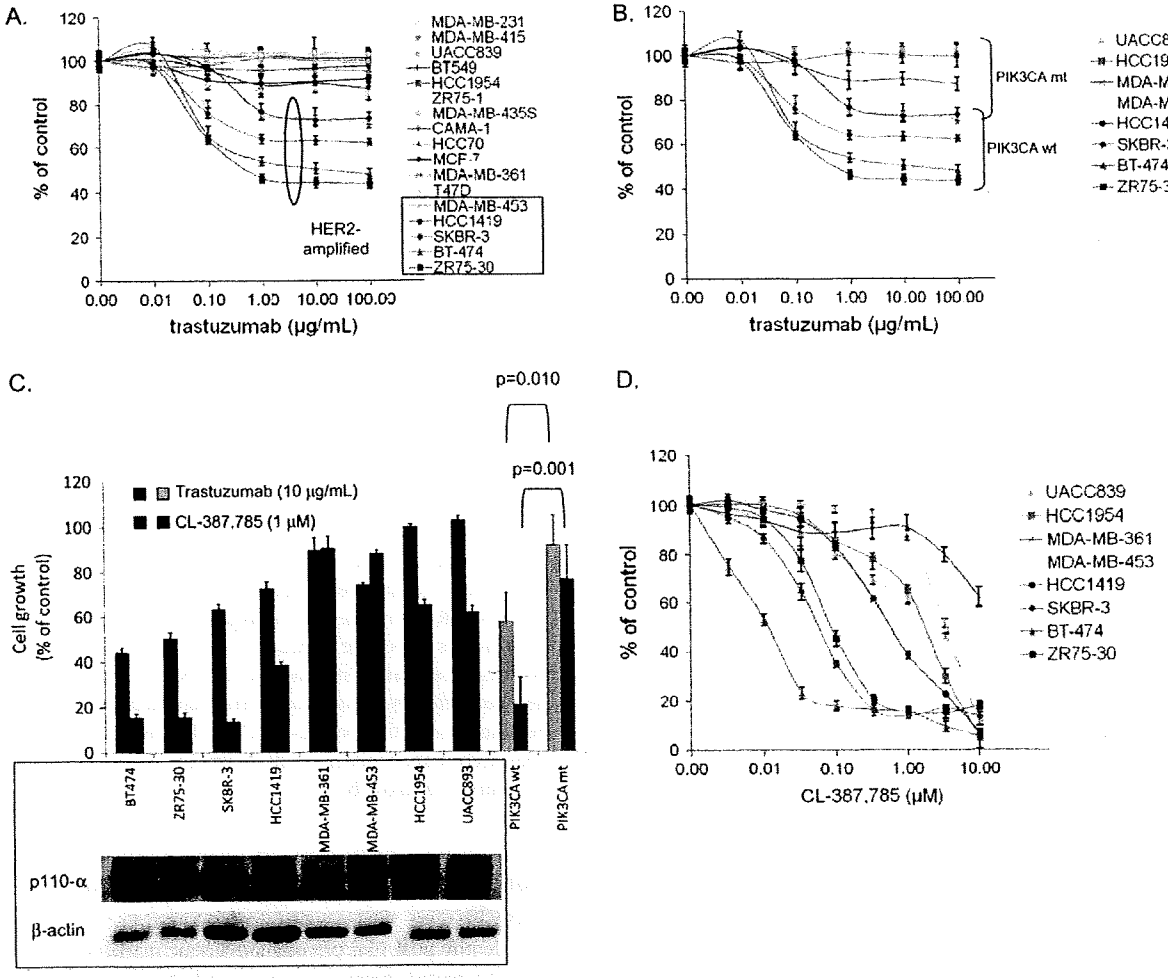

Figure 2. Effect of trastuzumab and CL-387,785 on growth inhibition in breast cancer cells *in vitro* [(**A**) trastuzumab on 17 breast cancer cell lines; (**B**) and (**D**) trastuzumab and CL-387,785 on eight *HER2*-amplified cell lines, respectively]. Breast cancer cells were grown in 10% serum-containing media for 5 days in the presence of various concentrations of trastuzumab (**A** and **B**) or CL-387,785 (**D**). The percentage of viable cells is shown relative to that of the untreated control and plotted on the *y*-axis, whereas trastuzumab and CL-387,785 concentrations are plotted on the *x*-axis. Each data point represents the mean value and standard deviation of 6–12 replicate wells. (**C**, top) Mean percentage of control and standard deviation of 6–12 replicate wells treated with 10 μg/ml trastuzumab and 1 μM CL-387,785, as well as those of *PIK3CA*-wild-type and -mutant cell lines (bottom), were plotted. (**C**, bottom) Protein expression of p110-α in *HER2*-amplified breast cancer cells. Blots were stripped and re-probed for β-actin as loading control.

Phosphorylation signals were then quantified and correlated with growth inhibition caused by trastuzumab and CL-387,785. As shown in Figure 4B, the closest association was observed between phospho-S6K changes and growth inhibition caused by trastuzumab and CL-387,785 [correlation coefficient (r), 0.811]. Further, close associations between phospho-S6K and cell growth were consistent when analyzed for trastuzumab and CL-387,785 separately (r for phospho-S6K versus growth: 0.8487 and 0.6970 for trastuzumab and CL-387,785, respectively).

dependency of *HER2*-amplified breast cancer cells on PI3K pathway

Given that inhibition of the PI3K pathway is critical in distinguishing cells sensitive from resistant to HER2-targeted agents (Figure 4B), we evaluated cell lines for the effects of LY294002, a PI3K inhibitor. As shown in Figure 5A, with the exception of ZR75-30, LY294002 induced a >30% growth inhibition compared with control in all cell lines. No significant difference in LY294002 sensitivity was observed between *PIK3CA*-mutant and -wild-type cell lines (Figure 5; $P = 0.655$). These results indicate that most *HER2*-amplified cells at least partly depend on the PI3K pathway regardless of the presence or absence of *PIK3CA* hotspot mutations.

To further gain insight into this concept, we evaluated phosphorylation levels of Akt and ERK1/2 in protein extracts obtained from cells under serum-starved conditions for 24 h. As shown in Figure 5B, despite the absence of serum factors, all *HER2*-amplified breast cancer cells showed a high level of phospho-Akt, regardless of *PIK3CA* genotype. High levels of phospho-Akt were also observed in MDA-MB-468, which lacks PTEN [30], and T47D, which harbors a *PIK3CA* mutation

(H1047R) [14]. These two cell lines do not show *HER2* amplification [23]. In contrast, no significant levels of phospho-Akt were observed in MDA-MB-231 and MDA-MB-435S, which show no *HER2* amplification, *PIK3CA* mutation, or PTEN loss [14, 23]. Further, with the exception of MDA-MB-231, all cell lines showed very low levels of phospho-ERK1/2 under serum-starved conditions. MDA-MB-231, in particular, was reported to contain double activating mutations in KRAS (G13D) and BRAF (G464V), whereas MDA-MB-435S showed an activating mutation in BRAF alone (V600E) [31]. These findings further support the concept that *HER2*-amplified cells tend to have HER2-PI3K signaling axis and they are thus dependent on the PI3K pathway rather than on extracellular signal-regulated kinase pathway.

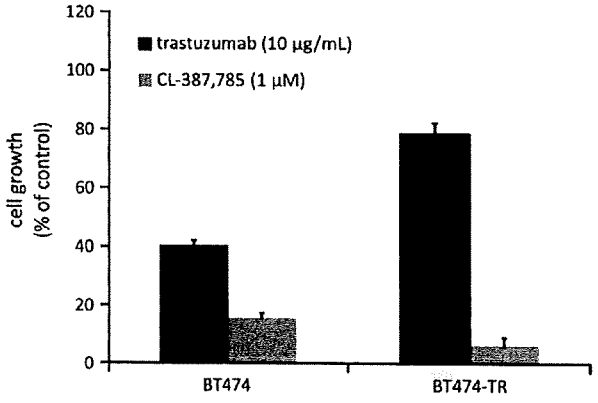

Figure 3. Effect of trastuzumab and CL-387,785 on growth inhibition in BT-474 and BT474-TR cells. Mean percentage of control and standard deviation of 6–12 replicate wells treated with 10 μg/ml trastuzumab and 1 μM CL-387,785 were plotted. BT474-TR remains sensitive to CL-387,785.

discussion

In this study, we show that gain-of-function mutations in *PIK3CA* genes are associated with trastuzumab resistance in naturally derived breast cancer cell lines showing *HER2* amplification. This finding is consistent with a recent study by Berns et al. [19] reporting trastuzumab resistance in SKBR-3 cells transfected with mutant *PIK3CA* (H1047R) compared with GFP control. Transfection of wild-type *PIK3CA*, however, appeared to equally cause trastuzumab resistance [19]. This observation does not identify either quantitative or qualitative changes in *PIK3CA* mutation as the major factor in developing trastuzumab resistance. In the present study, no clear association was observed between *PIK3CA* protein (p110-α) expression levels and *in vitro* sensitivity to trastuzumab

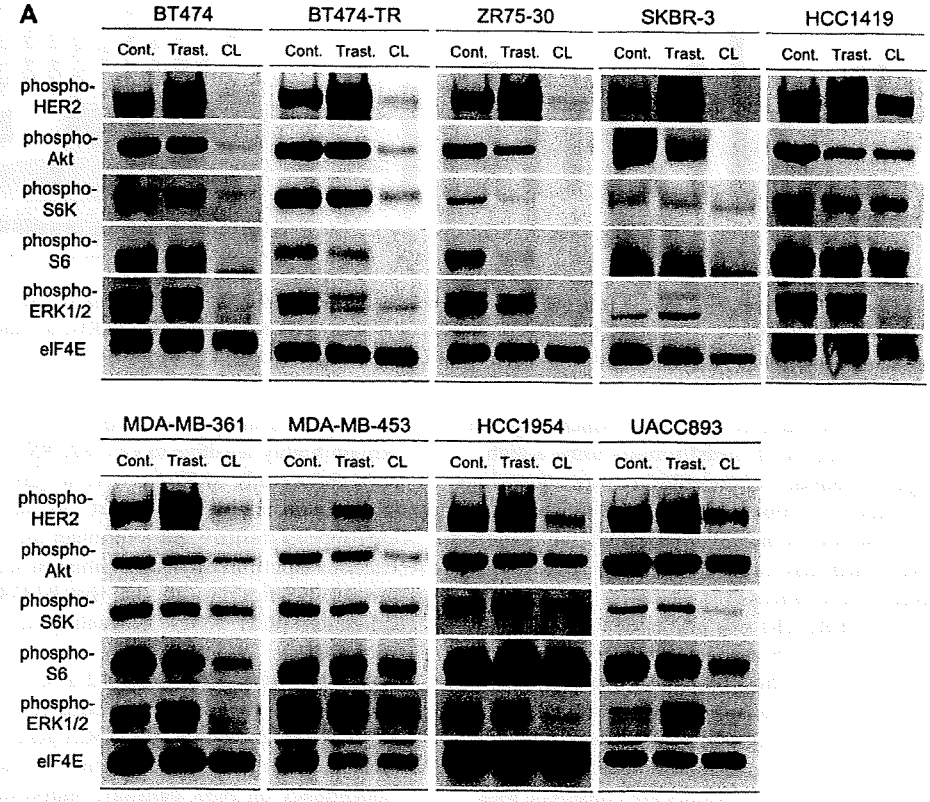

Figure 4. (A) Expression of phosphorylated-HER2, -Akt, -S6K, -S6 and -ERK1/2 in HER2-amplified breast cell lines with and without treatment with trastuzumab (10 μg/ml) and CL-387,785 (1 μM). Breast cell lines grown in 10% serum-containing media were lysed and immunoblotted for each protein. Blots were stripped and re-probed for eIF4E as loading control.

doi:10.1093/annonc/mdp304

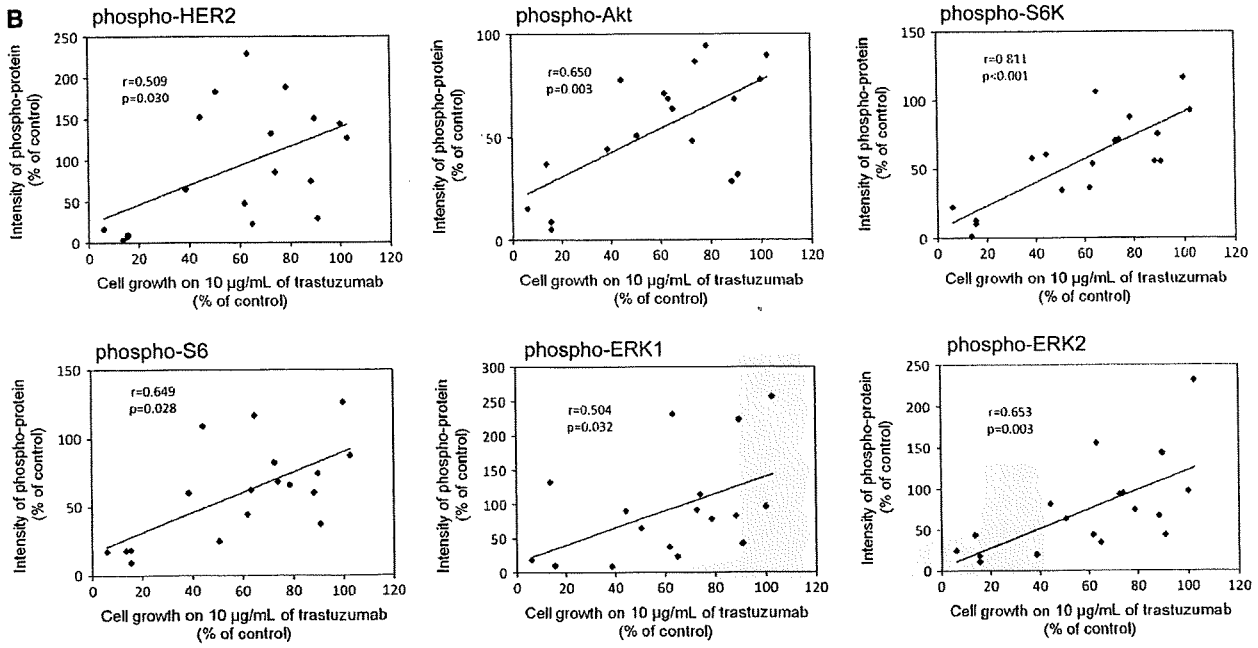

Figure 4. (Continued) (B) Correlation between changes in phosphorylation of HER2 signaling molecules and cell growth. Immunoblot quantification was carried out by densitometry using ImageJ software. Correlations were analyzed by calculating Pearson's correlation coefficient.

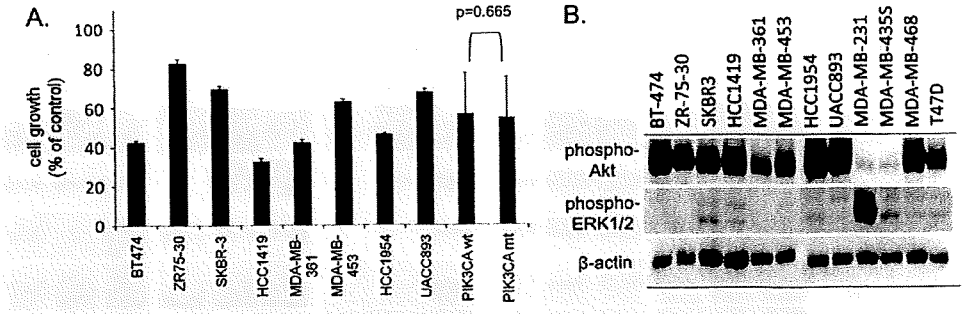

Figure 5. (A) Effect of LY294002 on growth inhibition in HER2-amplified breast cancer cell lines. Mean percentage of control and standard deviation of 6–12 replicate wells treated with 10 μM LY294002 were plotted. (B) Protein expression of phospho-Akt and phospho-ERK1/2 in HER2-amplified breast cancer cells under serum-starved condition. Blots were stripped and re-probed for β-actin as loading control.

(Figure 2C). A study by Haverty et al. [32], which analyzed copy number alterations in 51 breast tumors using a high-resolution single nucleotide polymorphism array, showed no gain in copy number on chromosome 3p, the location of the *PIK3CA* gene. These results indicate that qualitative changes in the *PIK3CA* gene itself may cause trastuzumab resistance in naturally derived breast cancer cells.

The CL-387,785 HER2-TKI was first evaluated to identify groups of compounds which may overcome trastuzumab resistance. Of note, results show an association between *PIK3CA* hotspot mutations and CL-387,785 resistance. Further, the difference in sensitivity between *PIK3CA*-wild-type and -mutant cell lines was more significant for CL-387,785 than for trastuzumab (Figure 2C). These results are consistent with a recent study by Eichhorn et al. [22], which showed that transfection of mutant *PIK3CA* (H1047R) in BT474 cells, which are sensitive to lapatinib, results in drug resistance. In contrast, the results of the present study show that BT474-TR cells remain highly sensitive to CL-387,785, which is consistent with a previous study by Konecny et al. [20] which reported that lapatinib remains active against cell lines selected by long-term exposure to trastuzumab. Although the study did not show the effect of lapatinib on cell signaling in secondary resistant cells, our present findings indicate that BT474-TR remains dependent on HER2/PI3K signaling and sensitive to HER2-TKI (Figure 4A).

We then evaluated LY294002 as a model PI3K inhibitor. Results show that *HER2*-amplified cells are generally sensitive to LY294002 regardless of *PIK3CA* genotype (Figure 5A), which indicates that *HER2* amplification is associated with dependency on PI3K pathway. Supporting this notion, all *HER2*-amplified breast cancer cells have high level of phosphorylation of Akt even in serum-starved condition. The Akt phosphorylation levels observed in *HER2*-amplified cells

were equivalent to those in MDA-MB-468 and T47D cells, which were reported to contain PTEN loss and a *PIK3CA* hotspot mutation without *HER2* amplification, respectively [23]. These findings therefore indicated that *HER2* amplification itself may have equivalent biological effect on PI3K signaling with PTEN loss or *PIK3CA* hotspot mutation. In addition, our results are consistent with a recent study by Oda et al. [33], in which they showed that HER2 and/or HER3 overexpression, PTEN, or *PIK3CA* mutations occur almost exclusively in breast and other cancer cell lines.

Findings in past and present studies may potentially lead to beneficial clinical applications. For *HER2*-amplified breast cancer showing no *PIK3CA* mutations, trastuzumab is likely to be effective, with possible rescue using HER2-TKIs in cases of relapse. For *HER2*-amplified breast cancer with *PIK3CA* mutations, inhibitors against molecules of the PI3K pathway are possibly more effective than anti-HER2 agents, which are unlikely to be beneficial.

In addition to pharmacogenetic approaches, including *PIK3CA* genotyping, pharmacodynamic markers are potentially powerful tools in individualized use of molecularly targeted therapy. In a number of previous pharmacodynamic studies on HER2- or EGFR-targeted therapy, phospho-Akt was used as a surrogate marker for PI3K pathway activity [34, 35]. In the present study, however, growth inhibition is more closely associated with changes in phospho-S6K than that in phospho-Akt. These findings indicate that the prediction of tumor response to trastuzumab may strongly benefit from measurements of S6K phosphorylation levels. The cause of the discrepancy between the association of cell growth with phospho-Akt and that with phospho-S6K, however, remains unclear. It may be due to the difference in sensitivity of phospho-specific antibodies used in the present study or the higher sensitivity of phospho-Akt to positive feedback signals following initial inhibition of the PI3K pathway compared with phospho-S6K.

The present study shows several limitations. First, although a relatively large panel of *HER2*-amplified breast cancer cell lines ($N = 8$) were used, the properties of all HER2-overexpressing breast tumors are not necessarily represented. Despite HER2 amplification being retained, particular tumor subtypes may have been selected in the establishment of cell lines. Secondly, in addition to inhibition of HER2 signaling, a few studies have indicated the contribution of antigen-dependent cellular cytotoxicity (ADCC) in the antitumor effect of trastuzumab. Because ADCC only works in *in vivo* conditions, our current data do not necessarily deny the potential effect of trastuzumab on tumors showing *PIK3CA* mutations [36]. Thirdly, although wild-type *PIK3CA* appeared necessary for trastuzumab sensitivity *in vitro*, other factors may be involved, as shown by results showing moderate resistance of HCC1419 to trastuzumab (Figure 2C). The mechanisms of *PIK3CA*-unrelated resistance remain unknown but are under current investigation in our laboratory.

In conclusion, our findings show an association between the presence of *PIK3CA* hotspot mutations and resistance to not only trastuzumab but also HER2-TKI in naturally derived *HER2*-amplified breast cancer cell lines. Further, PI3K inhibitors are potentially effective in overcoming trastuzumab resistance caused by *PIK3CA* mutations. Assessment of S6K phosphorylation levels may be a useful pharmacodynamic marker correlated to the antitumor effect of HER2-targeted therapy. A better understanding of these findings, however, may require further investigation in clinical trials and concomitant translational studies.

funding

Grant-in-Aid for Young Scientists (B) from Ministry of Education, Culture, Sports, Science and Technology of Japan to T.M.; AstraZeneca Research Grant 2007 to T.M.; Kobe University Medical School Research Grant for Young Scientists to T.M.; Grants-in-Aid for Cancer Research from Ministry of Health, Labor and Welfare of Japan to H.M.

references

1. McPherson K, Steel CM, Dixon JM. ABC of breast diseases. Breast cancer-epidemiology, risk factors, and genetics. BMJ 2000; 321: 624–628.
2. Parkin DM, Bray F, Ferlay J, Pisani P. Global cancer statistics, 2002. CA Cancer J Clin 2005; 55: 74–108.
3. Slamon DJ, Godolphin W, Jones LA et al. Studies of the HER-2/neu proto-oncogene in human breast and ovarian cancer. Science 1989; 244: 707–712.
4. Slamon DJ, Clark GM, Wong SG et al. Human breast cancer: correlation of relapse and survival with amplification of the HER-2/neu oncogene. Science 1987; 235: 177–182.
5. Slamon DJ, Leyland-Jones B, Shak S et al. Use of chemotherapy plus a monoclonal antibody against HER2 for metastatic breast cancer that overexpresses HER2. N Engl J Med 2001; 344: 783–792.
6. Piccart-Gebhart MJ, Procter M, Leyland-Jones B et al. Trastuzumab after adjuvant chemotherapy in HER2-positive breast cancer. N Engl J Med 2005; 353: 1659–1672.
7. Romond EH, Perez EA, Bryant J et al. Trastuzumab plus adjuvant chemotherapy for operable HER2-positive breast cancer. N Engl J Med 2005; 353: 1673–1684.
8. Buzdar AU, Ibrahim NK, Francis D et al. Significantly higher pathologic complete remission rate after neoadjuvant therapy with trastuzumab, paclitaxel, and epirubicin chemotherapy: results of a randomized trial in human epidermal growth factor receptor 2-positive operable breast cancer. J Clin Oncol 2005; 23: 3676–3685.
9. Vogel CL, Cobleigh MA, Tripathy D et al. Efficacy and safety of trastuzumab as a single agent in first-line treatment of HER2-overexpressing metastatic breast cancer. J Clin Oncol 2002; 20: 719–726.
10. Scaltriti M, Rojo F, Ocana A et al. Expression of p95HER2, a truncated form of the HER2 receptor, and response to anti-HER2 therapies in breast cancer. J Natl Cancer Inst 2007; 99: 628–638.
11. Xia W, Liu LH, Ho P, Spector NL. Truncated ErbB2 receptor (p95ErbB2) is regulated by heregulin through heterodimer formation with ErbB3 yet remains sensitive to the dual EGFR/ErbB2 kinase inhibitor GW572016. Oncogene 2004; 23: 646–653.
12. Nagata Y, Lan KH, Zhou X et al. PTEN activation contributes to tumor inhibition by trastuzumab, and loss of PTEN predicts trastuzumab resistance in patients. Cancer Cell 2004; 6: 117–127.
13. Samuels Y, Wang Z, Bardelli A et al. High frequency of mutations of the PIK3CA gene in human cancers. Science 2004; 304: 554.
14. Saal LH, Holm K, Maurer M et al. PIK3CA mutations correlate with hormone receptors, node metastasis, and ERBB2, and are mutually exclusive with PTEN loss in human breast carcinoma. Cancer Res 2005; 65: 2554–2559.
15. Campbell IG, Russell SE, Choong DY et al. Mutation of the PIK3CA gene in ovarian and breast cancer. Cancer Res 2004; 64: 7678–7681.
16. Lee JW, Soung YH, Kim SY et al. PIK3CA gene is frequently mutated in breast carcinomas and hepatocellular carcinomas. Oncogene 2005; 24: 1477–1480.
17. Isakoff SJ, Engelman JA, Irie HY et al. Breast cancer-associated PIK3CA mutations are oncogenic in mammary epithelial cells. Cancer Res 2005; 65: 10992–11000.

18. Gymnopoulos M, Elsliger MA, Vogt PK. Rare cancer-specific mutations in PIK3CA show gain of function. Proc Natl Acad Sci U S A 2007; 104: 5569–5574.
19. Berns K, Horlings HM, Hennessy BT et al. A functional genetic approach identifies the PI3K pathway as a major determinant of trastuzumab resistance in breast cancer. Cancer Cell 2007; 12: 395–402.
20. Konecny GE, Pegram MD, Venkatesan N et al. Activity of the dual kinase inhibitor lapatinib (GW572016) against HER-2-overexpressing and trastuzumab-treated breast cancer cells. Cancer Res 2006; 66: 1630–1639.
21. Cameron D, Casey M, Press M et al. A phase III randomized comparison of lapatinib plus capecitabine versus capecitabine alone in women with advanced breast cancer that has progressed on trastuzumab: updated efficacy and biomarker analyses. Breast Cancer Res Treat 2008; 112: 533–543.
22. Eichhorn PJ, Gili M, Scaltriti M et al. Phosphatidylinositol 3-kinase hyperactivation results in lapatinib resistance that is reversed by the mTOR/phosphatidylinositol 3-kinase inhibitor NVP-BEZ235. Cancer Res 2008; 68: 9221–9230.
23. Lacroix M, Leclercq G. Relevance of breast cancer cell lines as models for breast tumours: an update. Breast Cancer Res Treat 2004; 83: 249–289.
24. Mukohara T, Shimada H, Ogasawara N et al. Sensitivity of breast cancer cell lines to the novel insulin-like growth factor-1 receptor (IGF-1R) inhibitor NVP-AEW541 is dependent on the level of IRS-1 expression. Cancer Lett 2009; 282: 14–24.
25. Discafani CM, Carroll ML, Floyd MB Jr et al. Irreversible inhibition of epidermal growth factor receptor tyrosine kinase with in vivo activity by N-[4-[(3-bromophenyl)amino]-6-quinazolinyl]-2-butynamide (CL-387,785). Biochem Pharmacol 1999; 57: 917–925.
26. Zhang H, Liu G, Dziubinski M et al. Comprehensive analysis of oncogenic effects of PIK3CA mutations in human mammary epithelial cells. Breast Cancer Res Treat 2008; 112: 217–227.
27. Burris HA III, Hurwitz HI, Dees EC et al. Phase I safety, pharmacokinetics, and clinical activity study of lapatinib (GW572016), a reversible dual inhibitor of epidermal growth factor receptor tyrosine kinases, in heavily pretreated patients with metastatic carcinomas. J Clin Oncol 2005; 23: 5305–5313.
28. Shimamura T, Li D, Ji H et al. Hsp90 inhibition suppresses mutant EGFR-T790M signaling and overcomes kinase inhibitor resistance. Cancer Res 2008; 68: 5827–5838.
29. Koivunen JP, Mermel C, Zejnullahu K et al. EML4-ALK fusion gene and efficacy of an ALK kinase inhibitor in lung cancer. Clin Cancer Res 2008; 14: 4275–4283.
30. Stemke-Hale K, Gonzalez-Angulo AM, Lluch A et al. An integrative genomic and proteomic analysis of PIK3CA, PTEN, and AKT mutations in breast cancer. Cancer Res 2008; 68: 6084–6091.
31. Hollestelle A, Elstrodt F, Nagel JH et al. Phosphatidylinositol-3-OH kinase or RAS pathway mutations in human breast cancer cell lines. Mol Cancer Res 2007; 5: 195–201.
32. Haverty PM, Fridlyand J, Li L et al. High-resolution genomic and expression analyses of copy number alterations in breast tumors. Genes Chromosomes Cancer 2008; 47: 530–542.
33. Oda K, Okada J, Timmerman L et al. PIK3CA cooperates with other phosphatidylinositol 3′-kinase pathway mutations to effect oncogenic transformation. Cancer Res 2008; 68: 8127–8136.
34. Baselga J, Albanell J, Ruiz A et al. Phase II and tumor pharmacodynamic study of gefitinib in patients with advanced breast cancer. J Clin Oncol 2005; 23: 5323–5333.
35. Mohsin SK, Weiss HL, Gutierrez MC et al. Neoadjuvant trastuzumab induces apoptosis in primary breast cancers. J Clin Oncol 2005; 23: 2460–2468.
36. Clynes RA, Towers TL, Presta LG, Ravetch JV. Inhibitory Fc receptors modulate in vivo cytotoxicity against tumor targets. Nat Med 2000; 6: 443–446.

Cancer Letters 282 (2009) 14–24

Contents lists available at ScienceDirect

Cancer Letters

journal homepage: www.elsevier.com/locate/canlet

Sensitivity of breast cancer cell lines to the novel insulin-like growth factor-1 receptor (IGF-1R) inhibitor NVP-AEW541 is dependent on the level of IRS-1 expression

Toru Mukohara [a,b,*,1], Hiroyuki Shimada [b], Naomi Ogasawara [b], Ryoko Wanikawa [b], Manami Shimomura [b], Tetsuya Nakatsura [b], Genichiro Ishii [b], Joon Oh Park [d,e], Pasi A. Jänne [e], Nagahiro Saijo [b,c], Hironobu Minami [a,b,1]

[a] Division of Oncology and Hematology, National Cancer Center Hospital East, 6-5-1 Kashiwanoha, Kashiwa 277-8577, Japan
[b] Research Center for Innovative Oncology, National Cancer Center Hospital East, 6-5-1 Kashiwanoha, Kashiwa 277-8577, Japan
[c] Division of Thoracic Oncology, National Cancer Center Hospital East, 6-5-1 Kashiwanoha, Kashiwa 277-8577, Japan
[d] Division of Hematology–Oncology, Department of Medicine, Samsung Medical Center, Sungkyunkwan University, School of Medicine, 50 Irwon-Dong, Gangnam-Gu, Seoul 135-710, Republic of Korea
[e] Lowe Center for Thoracic Oncology, Department of Medical Oncology, Dana-Farber Cancer Institute, 44 Binney Street, Boston, MA 02115, USA

ARTICLE INFO

Article history:
Received 3 June 2008
Received in revised form 27 November 2008
Accepted 25 February 2009

Keywords:
Breast cancer
IGF-1R
IRS-1
Tyrosine kinase inhibitor

ABSTRACT

To investigate the potential value of targeting insulin-like growth factor-1 receptor (IGF-1R) in breast cancer, we examined the effects of NVP-AEW541, a selective small-molecule inhibitor of the IGF-1R tyrosine kinase, in a panel of 16 breast cancer cell lines. All cell lines expressed IGF-1R, but MCF-7 expressed much higher levels of insulin receptor substrate-1 (IRS-1) than the others. NVP-AEW541 was more potent at inhibiting growth of MCF-7 cells as compared to the others (IC_{50}, 1 μM vs. ≈7 μM). Comparing MCF-7 to T47D cells, which express IGF-1R at a level identical to MCF-7 but have less than 1/30 the amount of IRS-1, NVP-AEW541 caused cell-cycle arrest at the G1–S boundary, reduced *in vitro* cell migration, and enhanced the cytotoxic effects of vinorelbine and paclitaxel in MCF-7, but not in T47D. While NVP-AEW541 decreased the phosphorylation of IGF-1R in both cell lines, it inhibited phosphorylation of Akt and disrupted the IRS-1/PI3 K complex only in MCF-7. These findings suggest that inhibiting IGF-1R may be an effective therapeutic strategy for breast cancers that co-express IGF-1R and IRS-1 at high levels.

1. Introduction

With approximately a million new cases annually, breast cancer is the leading cause of cancer death among women worldwide [1,2]. Once the disease metastasizes, it is no longer curable despite use of various systemic treatments including cytotoxic chemotherapies, endocrine manipulations, and anti-HER2 monoclonal antibodies. Therefore, novel therapeutic approaches are needed.

Since 1990s, molecularly-targeted drugs have been vigorously developed for cancer treatment. Today, receptor tyrosine kinases (RTKs) are the most promising therapeutic targets. In fact trastuzumab, an anti-HER2 monoclonal antibody used to treat HER2-overexpressing breast cancers, was one of the first therapeutic agents targeting RTKs in solid tumors. For treatment of HER2-overexpressing metastatic breast cancers, trastuzumab combined with conventional chemotherapy has significantly higher efficacy than chemotherapy alone [3]. The use of trastuzumab has recently been extended to adjuvant or neo-adjuvant

* Corresponding author. Tel.: +81 78 382 5825; fax: +81 78 382 5821.
E-mail address: mukohara@med.kobe-u.ac.jp (T. Mukohara).
[1] Present address: Department of Medical Oncology, Kobe University Hospital, 7-5-1, Kusunoki-cho, Chuo-ku, Kobe 650-0017, Japan.

0304-3835/$ - see front matter © 2009 Elsevier Ireland Ltd. All rights reserved.
doi:10.1016/j.canlet.2009.02.056

treatment for operable breast cancer [4–6]. Among other solid tumors, small-molecule tyrosine kinase inhibitors of epidermal growth factor receptor (EGFR) and Kit have provided new treatment options in patients with non-small cell lung cancer and gastrointestinal stromal tumor, respectively [7].

Insulin-like growth factor-1 receptor (IGF-1R) is another RTK characterized by its contribution to a variety of oncogenic properties, including cell proliferation, cell survival, cell motility, angiogenesis, and metastasis [8–10]. The ligands of IGF-1R are insulin-like growth factor-1 (IGF-1) and IGF-2. Once the ligands bind to IGF-1R's extracellular domain, the receptor is autophosphorylated and becomes active as a tyrosine kinase. Subsequently, adaptor molecules, such as insulin receptor substrate-1 (IRS-1) or IRS-2, are tyrosine-phosphorylated and mediate downstream signaling. This includes activation of the phosphatidylinositol 3-kinase (PI3 K)/Akt and Ras-Raf-MEK-ERK1/2 pathways [8,10]. In breast cancer cell lines, it was reported that IRS-1, but not IRS-2, is the predominant signaling molecule activated by IGF-1 [11]. Several mechanisms able to enhance the PI3 K pathway in malignancies have been identified. In breast cancer, these include mutation of p110, which is the catalytic subunit of PI3 K, and the loss of PTEN [12]. Recent studies suggested that these PI3 K-enhancing alterations may cause resistance to anti-RTK agents, such as trastuzumab and erlotinib [13–15].

Protein expression of IGF-1R is elevated in a majority of breast cancer cell lines and in 39–93% of breast cancer tumors [8,16]. Elevated levels of circulating IGF-1 have been found to be associated with an increased risk of developing breast cancer [17]. IRS-1 is reported to be frequently phosphorylated in breast cancer tumors [18] and the level of IRS-1 is correlated with shorter disease-free survival in a subgroup of breast cancer patients [19]. Further, Lu, et al. have proposed a potential mechanism of resistance to trastuzumab *in vitro*, which consists of alternative cell signaling triggered by IGF-1R instead of HER2 in the presence of trastuzumab [20]. Based on these findings, IGF-1R is considered to be a rational therapeutic target in breast cancer.

Several different methods for targeting IGF-1R are under investigation, including oligodeoxynucleotides, monoclonal antibodies, and small-molecule tyrosine kinase inhibitors [8]. Among these, small-molecule inhibitors have the advantage of possible oral administration. NVP-AEW541 is a selective inhibitor for IGF-1R tyrosine kinase [21,22]. A previous study showed that it inhibited anchorage-independent growth of MCF-7 breast cancer cells [22]. Here, as part of our investigations into protocol designs for clinical trials of NVP-AEW541 in patients with breast cancer, we evaluated the efficacy of this agent in a large panel of breast cancer cell lines, its activities against oncogenic processes other than cell growth, details of its mechanism of action, and methods for identifying tumors likely to respond to it.

In this study, we show that NVP-AEW541 inhibits cell growth and motility, and enhances the induction of apoptosis by chemotherapeutic agents *in vitro*. These effects were observed only in MCF-7 breast cancer cells, the only line among those tested that expresses both IGF-1R and IRS-1 at high level. We also showed that NVP-AEW541 inhibits Akt phosphorylation by causing dissociation of IRS-1/PI3 K complex, which appears to be an important mechanism of action. These results suggest that cells that co-express IGF-1R and IRS-1 are likely to be dependent on the signaling pathway from IGF-1R to PI3 K, and therefore sensitive to NVP-AEW541, which disrupts this pathway.

2. Materials and methods

2.1. Cell culture

MCF-7, MDA-MB-361, HCC1954, MDA-MB-453, UACC893, CAMA-1, MDA-MB-435S, ZR75-30, HCC70, and HCC1419 cell lines were purchased from the American Type Culture Collection (ATCC, Manassas, VA). BT474, SKBR-3, BT549, T47D, ZR75-1, and MDA-MB-231 cells were kindly provided by Dr. Ian Krop of the Dana-Farber Cancer Institute. MCF-7, HCC1954, MDA-MB-453, UACC893, CAMA-1, ZR75-30, HCC70, HCC1419, BT474, SKBR-3, BT549, T47D, and ZR75-1 cells were maintained in RPMI 1640 (Cellgro; Mediatech, Inc., Herndon, CA) supplemented with 10% FBS (Gemini-Bio-Products, Inc., Woodland, CA), 100 units/ml penicillin, 100 units/ml streptomycin, and 2 mM glutamine. MDA-MB-361, MDA-MB-435S, and MDA-MB-231 cells were maintained in Dulbecco's Modified Eagle's Medium (DMEM) (Cellgro) with 10% FBS, 100 units/ml penicillin, 100 units/ml streptomycin, and 2 mM glutamine.

2.2. Drugs

NVP-AEW541 was a kind gift of Novartis Pharma (Basel, Switzerland). Stock solutions were prepared in dimethyl sulfoxide (DMSO) and stored at −20 °C. The drugs were diluted in fresh media before each experiment. In all experiments, the final concentration of DMSO was less than 0.1%. The lack of effect of DMSO at this concentration on cell growth, cell migration, or cell-cycle distribution in MCF-7 and T47D was confirmed (data not shown). Vinorelbine and paclitaxel were purchased from the pharmacy of the National Cancer Center Hospital East.

2.3. Antibodies and Western blotting

Cells were lysed in lysis buffer (20 mM Tris [pH 7.5], 150 mM NaCl, 10% glycerol, 1% NP40, and 2 mM EDTA) containing protease and phosphatase inhibitors (100 mM NaF, 1 mM phenylmethylsulfonyl fluoride [PMSF], 1 mM Na_3VO_4 2 μg/ml aprotinin, and 5 μg/ml leupetin). Cell lysates were centrifuged at 14,000*g* relative centrifugal force (rcf) to make protein extracts. The protein extracts were separated by gel electrophoresis on 7–10% polyacrylamide gels (depending on the target's molecular weight), transferred to nitrocellulose membranes (Schleicher and Schuell, Dassel, Germany) and detected by immunoblotting using Amersham ECL™ Advance Western Blotting Detection Kit (GE Healthcare, Buckinghamshire, England). The resulting signals were quantified to obtain digital values

using a GS-800 calibrated densitometer (Bio-Rad, Hercules, CA) and Quantity One 1-D analysis software (Bio-Rad). The phospho-IGF-1R (19H7, Tyr1135/1136), IGF-1R, phospho-IRS-1 (Ser 612), IRS-1, phospho-Akt (pS473), Akt, and PTEN antibodies were purchased from Cell Signaling Technology (Beverly, MA). The phospho-ERK1/2 (pT185/pY187) and ERK1/2 antibodies were purchased from Biosource International Inc (Camarillo, CA). The p85 antibody was purchased from Upstate (Charlottesville, VA). The β-actin antibody was purchased from Sigma–Aldrich (St. Louis, MO).

2.4. Phospho-RTK array

At approximately 70% of cell confluence, protein extracts of MCF-7, T47D, HCC1954, and MDA-MB-361 cells were prepared as described in Section 2.3. The extracts were applied to a Human Phospho-RTK Array (R&D Systems, Minneapolis, MN, USA), which can detect the phosphorylation level of 42 different RTKs on the same nitrocellulose membrane. Assays were performed in accordance with the manufacturer's instructions. The resulting signals were quantified as described in Section 2.3. The intensity of each RTK's phosphorylation was represented as a percentage relative to the internal positive control. To obtain relative intensity among the 42 RTKs, the deviation value was calculated as follows: (intensity for the RTK – average intensity for 42 RTKs) × 10/standard deviation of intensities for 42 RTKs.

2.5. Immunoprecipitation

Immunoprecipitation was performed as described previously [23]. Briefly, fresh protein extracts (see Section 2.3) were incubated overnight with anti-p85 antibody. Immunoprecipitation products were washed three times with ice-cold NP-40 lysis buffer before boiling in 2× Laemmli sample buffer and analyzed by Western blotting.

2.6. Cell growth assay

Growth inhibition was assessed by use of the MTS assay (Promega, Madison, WI). This assay, a colorimetric method for determining the number of viable cells, is based on the bioreduction of 3-(4,5-dimethylthiazol-2-yl)-5-(3-carboxymethoxyphenyl)-2-(4-sulfophenyl)-2H-tetrazolium (MTS) to a soluble formazan product that is detected spectrophotometrically at a wavelength of 490 nm. Cells diluted in 160 μl/well of maintenance cell culture media (see "*Cell Culture and Reagents*") were plated in 96-well flat-bottom plates (Corning, Inc., Corning, NY). The number of cells required to obtain an optical density (OD) of 1.3–2.2, the linear range of the assay, after 96 h of growth was determined for each cell line beforehand. The number

Table 1
Baseline expression of phospho-IGF-1R, IGF-1R, phospho-IRS-1, and IRS-1 in breast cancer cells grown in 10% serum-containing media.

	Phospho-IGF-1R	IGF-1R	Phospho-IRS-1	IRS-1
BT474	0.34	0.47	0.10	0.11
BT549	0.28	0.26	0.06	0.07
CAMA-1	0.22	0.00	0.04	0.00
HCC1419	0.61	0.35	0.04	0.09
HCC1954	2.48	0.49	0.08	0.20
HCC70	0.19	0.57	0.14	0.15
MCF-7	1.00	1.00	1.00	1.00
MDA-MB-MB231	0.44	0.34	0.28	0.27
MDA-MB-MB361	1.72	0.95	0.11	0.05
MDA-MB-435S	0.54	0.85	0.11	0.10
MDA-MB-453	0.05	0.25	0.08	0.05
SKBR-3	0.86	0.41	0.01	0.02
T47D	1.15	1.10	0.03	0.03
UACC893	0.28	0.57	0.01	0.01
ZR75-1	0.25	0.96	0.09	0.24
ZR75-30	0.38	0.40	0.01	0.02

Intensity of each band measured with Western blotting for each cell line (Fig. 1) was quantified and expressed relative to that for MCF-7.

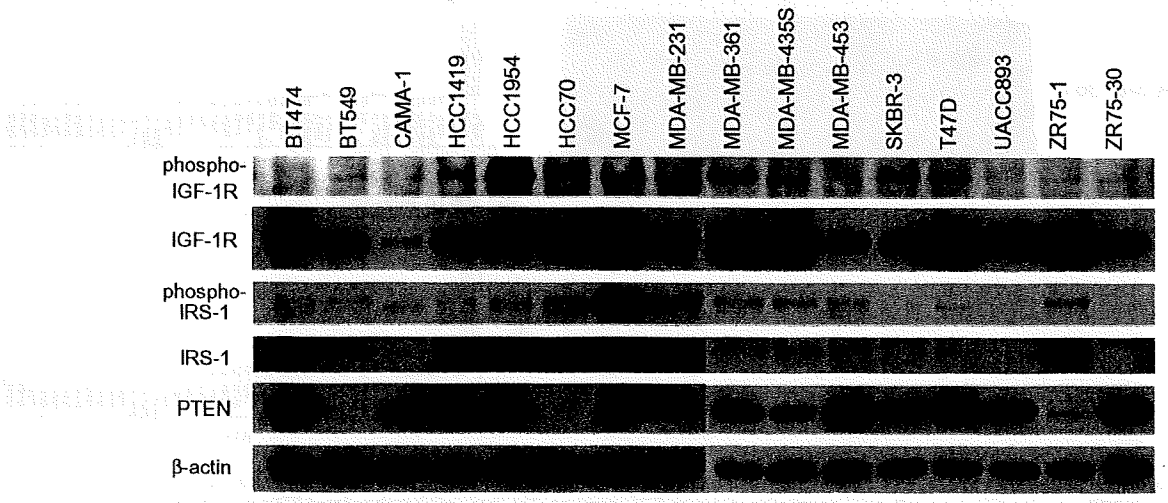

Fig. 1. Expression of phosphorylated IGF-1R, IGF-1R, phosphorylated IRS-1, IRS-1, and PTEN in breast cancer cell lines. Breast cancer cell lines grown in 10% serum-containing medium were lysed and immunoblotted for each protein. The blots were stripped and reprobed for β-actin as loading control.

of cells per well used in the subsequent experiments were as follows: MCF-7, 2000; MDA-MB-361, 8000; HCC1954, 2500; MDA-MB-453, 7000; UACC893, 7500; CAMA-1, 6000; MDA-MB-435S, 2000; ZR75-30, 7500; HCC70, 4000; HCC1419, 8000; BT474, 3000; SKBR-3, 2500; BT549, 2000; T47D, 2500; ZR75-1, 7500; and MDA-MB-231, 2500. Drugs were added 24 h after plating, and the cells were incubated for another 96 h. Wells of the plate (6–12) were set for each experimental point, and all experiments were repeated at least three times. The data are expressed as percentage of growth relative to that of untreated control cells.

2.7. FACS analysis

The FACS analysis was performed using methods similar to those described previously [24]. Briefly, 1–1.5 × 10^6 cells were seeded into 10 cm^3 plates, and the drugs were added 24 h later. After 24 h of treatment, the cells were trypsinized and fixed overnight in ethanol at 4 °C. Fixed cells were then resuspended in 0.5% RNase A (Sigma), centrifuged, resuspended in 5 μM propidium iodine (Sigma) in 38 mM sodium citrate, incubated at room temperature for 30 min, and analyzed by FACS Calibur flow cytometry (Becton Dickinson, Franklin Lakes, NJ) with a cell-cycle test software, ModFit LT™ (Verity Software House Inc., Topsham, ME). All experiments were repeated three times.

2.8. Scratch wound migration assay

Breast cancer cells were seeded in 6-well tissue culture plates (Corning, Inc.) and incubated in 10% serum-containing media until confluence. Gaps were then created by scraping cells with P1000 pipette tips and the cells were

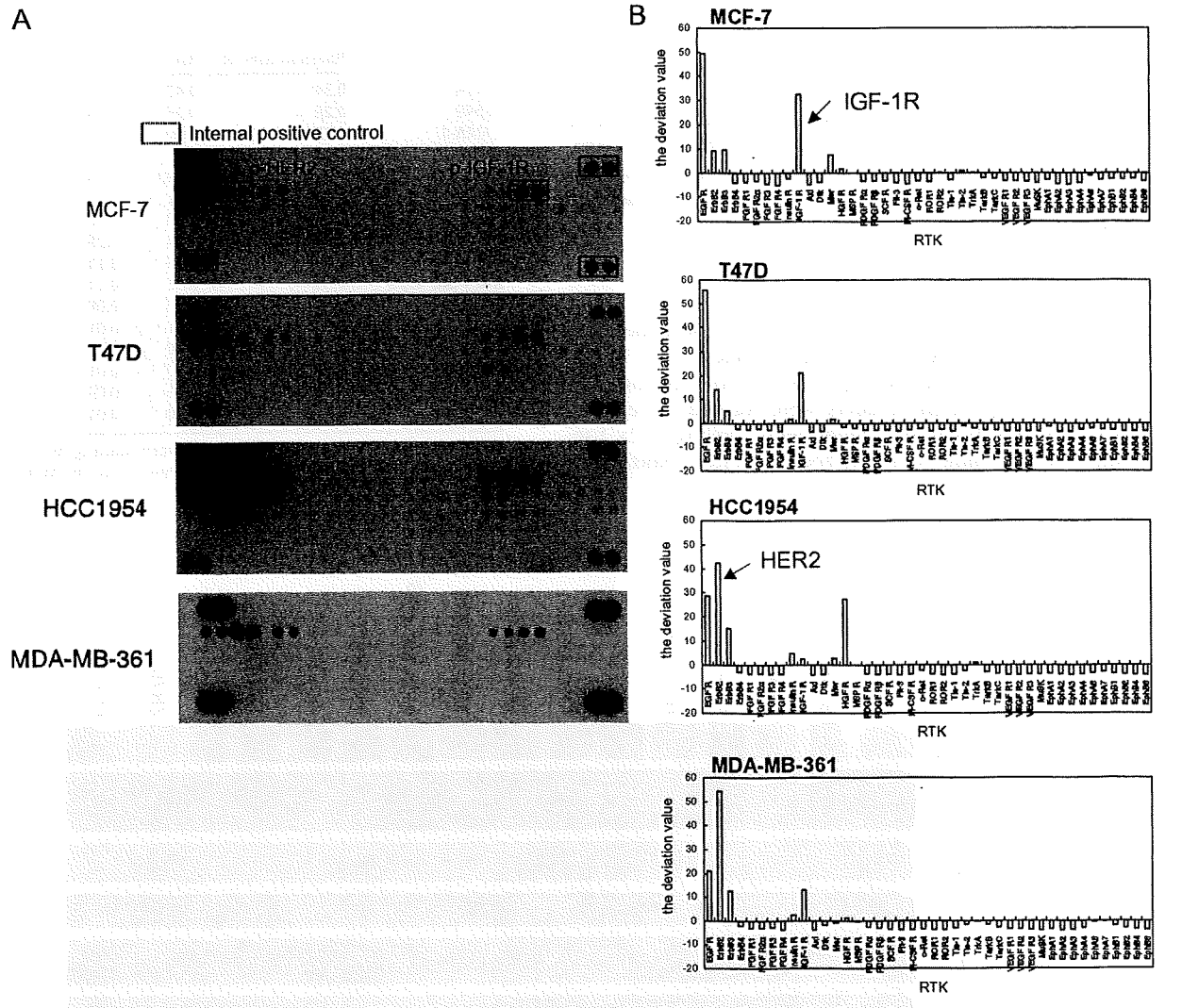

Fig. 2. Phosphorylation profile of 42 RTKs in MCF-7, T47D, HCC1954, and MDA-MB-361 breast cancer cell lines. The protein extract prepared from each cell line grown in 10% serum-containing medium was applied to phospho-RTK arrays. (A) The levels of phosphorylated RTKs in each cell line were visualized on a nitrocellulose membrane. (B) The average intensities of the dots for each phosphorylated RTK (*x*-axis) were quantified. The deviation value was calculated as described in Section 2 and plotted on the *y*-axis.

cultured in fresh media containing 10% serum with or without 1 μM NVP-AEW541. The plates were photographed at 0, 24, 48, 72, and 96 h using a microscope with a digital video camera installed (BZ-8000, Keyence, Osaka, Japan). Distance of cell migration was measured at three fixed positions (top, right middle and bottom on the screen) using BZ analyzer software (Keyence).

3. Results

3.1. Expression and phosphorylation level of IGF-1R and IRS-1 in breast cancer cell lines

Sixteen breast cancer cell lines were evaluated for the expression and phosphorylation level of IGF-1R and IRS-1 using Western blotting. All the lines expressed detectable levels of IGF-1R (Fig. 1). While a majority of them exhibited phosphorylation of IGF-1R detectable with the phospho-specific antibody, there was no clear correlation between expression level and phosphorylation of the receptor (Fig. 1 and Table 1, $p = 0.07$). On the other hand, expression and phosphorylation level of IRS-1 appeared significantly correlated with each other (Fig. 1 and Table 1, $p = 0.002$). MCF-7 cells expressed substantially more IRS-1 and phospho-IRS-1 than the other 15 cell lines, with levels at least three times those seen in other lines (Fig. 1 and Table 1). Of the 16 breast cancer cell lines, all but BT549, HCC70, and ZR75-1 expressed detectable levels of PTEN (Fig. 1).

3.2. MCF-7 and T47D have high relative phosphorylation of IGF-1R

Fifty-eight RTKs have been identified in the human genome [25], and cancer cells could potentially depend on any RTK in terms of activating downstream effectors. To shed light on the relative importance of IGF-1R among many other RTKs in breast cancer cells, we utilized a commercially available phospho-RTK array, which can detect the phosphorylation level of 42 different RTKs on one nitrocellulose membrane (see Section 2). Protein extracts obtained from MCF-7, T47D, HCC1954, and MDA-MB-361 cells, which had the highest levels of phosphorylated IGF-1R as measured by Western blotting (Fig. 1 and Table 1), were applied to the array. We quantified each phospho-RTK as described in Section 2. As shown in Fig. 2, the relative intensity of phosphorylated IGF-1R is higher in MCF-7 and T47D than in HCC1954 and MDA-MB-361. Of note, both HCC1954 and MDA-MB-361 are reported to have amplification of the HER2 gene and over-expression of the protein [26]. Consistent with this, the relative intensity of phosphorylated HER2 is high in those two cell lines (Fig. 2).

3.3. NVP-AEW541 inhibits cell growth of breast cancer cell lines

To examine the inhibitory effects of NVP-AEW541 on cell growth, cells were cultured in 10% serum-containing media with various concentrations of NVP-AEW541 (3.3 nM to 10 μM). As seen in Fig. 3, NVP-AEW541 inhibits cell growth of MCF-7 more potently than that of the other breast cancer cell lines (IC_{50} for MCF-7 vs. the other cell lines, 1 μM vs. approximately. 7 μM).

Taken together, neither expression nor phosphorylation of IGF-1R predicts sensitivity to NVP-AEW541. This is shown by comparison of the MCF-7 and T47D cell lines, which showed different sensitivities to NVP-AEW541 despite equivalency in expression and phosphorylation level of IGF-1R (Figs. 1 and 3, and Table 1). In addition, those two cell lines have very similar phospho-RTK profiles as shown in Fig. 2. On the other hand, IRS-1 expression and phosphorylation levels are much higher in MCF-7 cells than in T47D cells (Fig. 1 and Table 1). To explore the role of IRS-1 in the mechanism of action of NVP-AEW541, we therefore decided to compare MCF-7 with T47D in further experiments. Because NVP-AEW541 can inhibit many other kinases, especially insulin receptor, at concentrations above 2 μM [22], we could not exclude the possibility that growth inhibition observed at 3.3 μM or higher might be due to non-specific effects. Therefore, we used 1 μM or lower concentrations of NVP-AEW541 in subsequent experiments.

3.4. NVP-AEW541 alters cell-cycle distribution

FACS analysis was used to determine the effect of NVP-AEW541 on MCF-7 and T47D cell cycling. In MCF-7 cells, treatment with 1 μM NVP-AEW541 led to an increase in the G1–G0 fraction along with a decrease in the G2–M and S fractions, indicating cell-cycle arrest at the G1–S boundary (Fig. 4A). In contrast, very little change in cell-cycle distribution was observed in T47D cells (Fig. 4B). NVP-AEW541 produced no increase

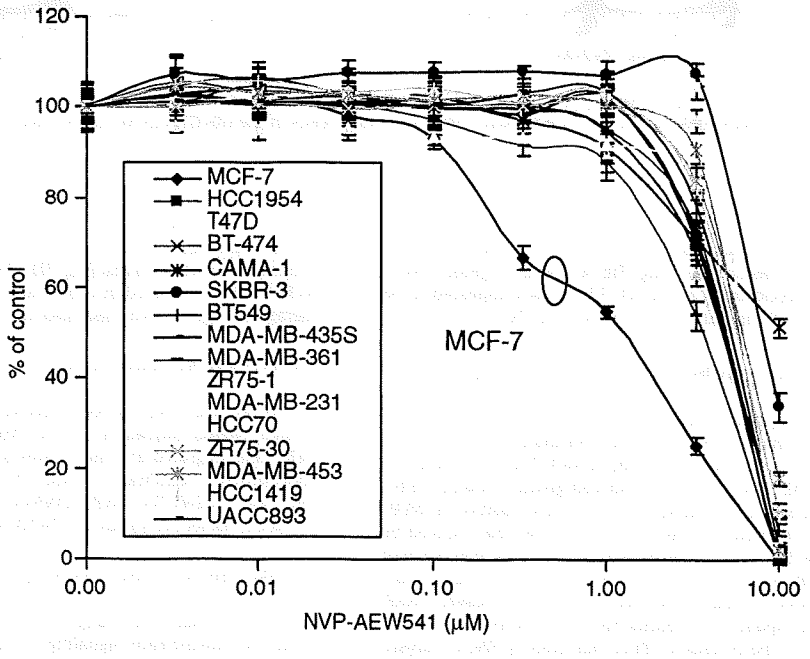

Fig. 3. Growth inhibitory effect of NVP-AEW541 on breast cancer cells. Breast cancer cells are grown in 10% serum-containing media for 5 days in the presence of various concentrations of NVP-AEW541. Percentage of viable cells is shown relative to that of untreated control (*y*-axis). The *x*-axis shows the concentration of NVP-AEW541. Each data point represents the mean value and standard deviation of 6–12 replicate wells.

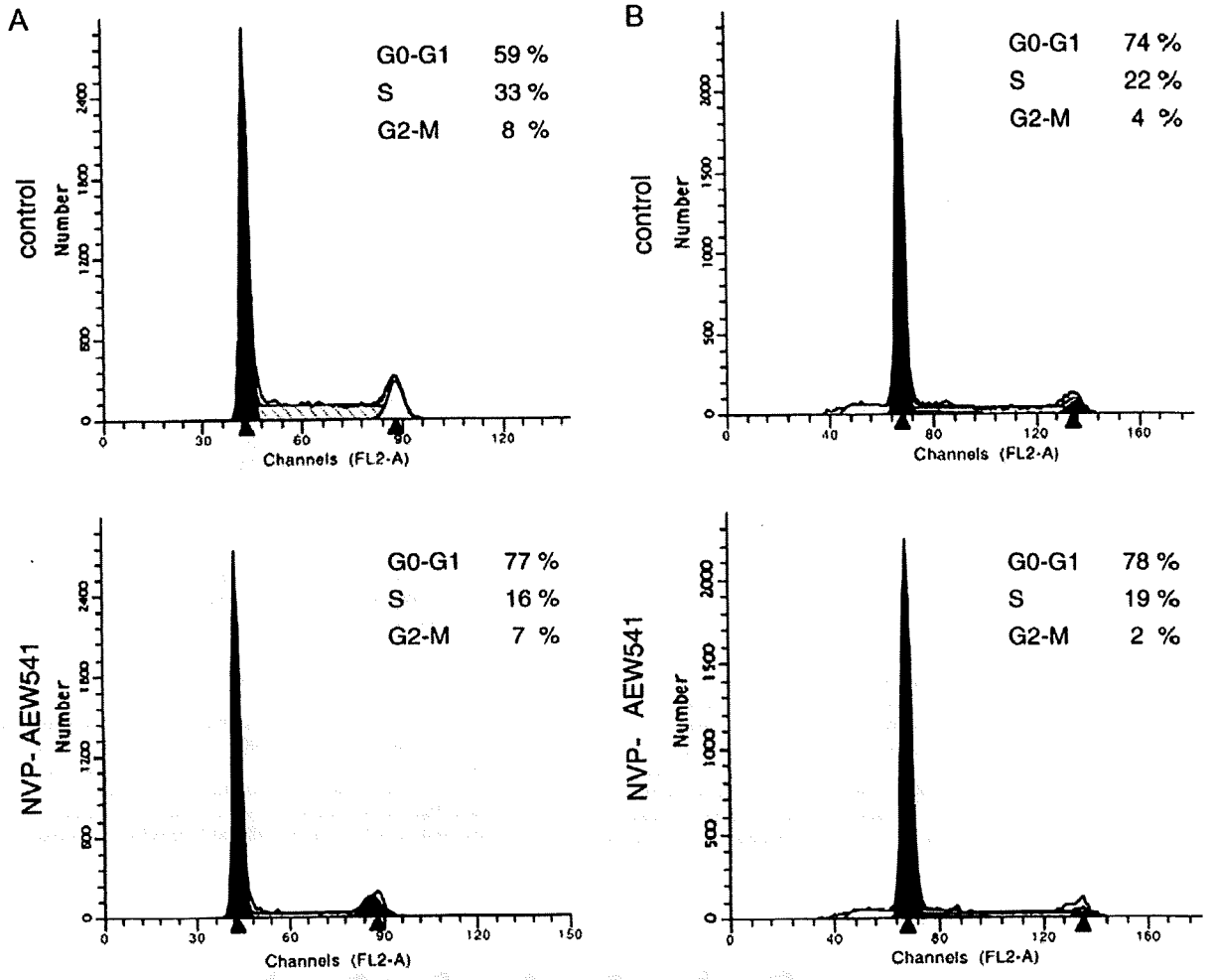

Fig. 4. Change in cell-cycle parameters in MCF-7 (A) and T47D (B) cells as a result of NVP-AEW541 treatment. Examples of FACS analysis of cells that were treated with 0 and 1 μM of NVP-AEW541 for 24 h are shown. The proportion of cells in the G0–G1, G2–M, and S phases of the cell-cycle are shown on top right hand corner.

in the sub-G1 fraction, indicative of apoptosis, in either cell line, suggesting a cytostatic effect of the drug (Fig. 4). Taken together, NVP-AEW541-induced cell-cycle arrest at the G1–S boundary appeared to be responsible for the growth inhibition seen in MCF-7 cells.

3.5. NVP-AEW541 enhances the effect of chemotherapeutic drugs

Because IGF-1R signaling is known to be important for cell survival [8], we next examined the ability of NVP-AEW541 to enhance cytotoxicity of chemotherapeutic agents. As seen in Fig. 5A, in MCF-7 a combination of vinorelbine and NVP-AEW541 generally produced greater growth inhibition than either drug alone. In contrast, in T47D cells, addition of NVP-AEW541 caused little increase in growth inhibition over that induced by vinorelbine alone (Fig. 5B). To evaluate the level of apoptosis, Western blot analysis for poly (ADP-ribose) polymerase (PARP) was performed. Treatment with NVP-AEW541 produced no clear increase in cleaved PARP, which is indicative for apoptosis, in either MCF-7 or T47D cells (Fig. 5C and D), consistent with the cytostatic effect indicated by FACS analysis. Treatment with vinorelbine caused an increase in cleaved PARP in both cell lines (Fig. 5C and D). In MCF-7 cells, the addition of NVP-AEW541 to vinorelbine caused a further increase, suggesting that the compound enhances vinorelbine-induced apoptosis (Fig. 5C), but in T47D cells the enhancement was minimal (Fig. 5D). Similar results were observed when NVP-AEW541 was used in combination with paclitaxel, another chemotherapeutic agent often used against breast cancer (data not shown).

3.6. NVP-AEW541 inhibits migration of MCF-7 cells

To test the effect of NVP-AEW541 on cell motility, we performed scratch wound migration assays. Without NVP-AEW541, MCF-7, and T47D cells migrated at similar rates over 96 h. Treatment with 1 μM of NVP-AEW541 significantly reduced the rate of migration in MCF-7 (Fig. 6A, control vs. NVP-AEW541 at 72 and 96 h, $p = 0.001$ and $P < 0.001$, respectively) but not T47D cells (Fig. 6B).

3.7. NVP-AEW541 inhibits IGF-1R signaling in MCF-7

We next examined changes in phosphorylation of IGF-1R and representative downstream signaling molecules in MCF-7 and T47D cells grown in 10% serum media with or without 1 μM NVP-AEW541. In both cell lines, NVP-AEW541 inhibited phosphorylation of IGF-1R (Fig. 7A). Baseline phospho-IRS-1 was much higher in MCF-7 cells than in T47D,